NASA TECHNICAL NOTE

NASA TN D-4887
ᶜ.1

EXPERIMENTAL STUDIES ON SHADOW SHIELDS FOR THERMAL PROTECTION OF CRYOGENIC TANKS IN SPACE

by Richard H. Knoll and Edward R. Bartoo

Lewis Research Center
Cleveland, Ohio

NATIONAL AERONAUTICS AND SPACE ADMINISTRATION • WASHINGTON, D. C. • NOVEMBER 1968

NASA TN D-4887

EXPERIMENTAL STUDIES ON SHADOW SHIELDS FOR THERMAL

PROTECTION OF CRYOGENIC TANKS IN SPACE

By Richard H. Knoll and Edward R. Bartoo

Lewis Research Center
Cleveland, Ohio

NATIONAL AERONAUTICS AND SPACE ADMINISTRATION

ABSTRACT

Experiments were performed on multiple flat-disk shadow shields to determine the effects of shield spacing, number, emissivity, lateral conductance, and targeting (high-emissivity coatings on annular rings of shields) on thermal performance. The experimental data, in general, agreed closely with an analytical model which assumed diffuse surfaces with nonuniform radiosity. A shadow-shield system for a hypothetical space vehicle was designed, scaled down, and tested. Results demonstrated: (1) a lightweight method of shield construction; (2) shield-support interactions; and (3) reduction of support heat leaks by shield location, attachment methods, and the use of high-emissivity coatings.

EXPERIMENTAL STUDIES ON SHADOW SHIELDS FOR THERMAL

PROTECTION OF CRYOGENIC TANKS IN SPACE

by Richard H. Knoll and Edward R. Bartoo

Lewis Research Center

SUMMARY

Experimental data were obtained on the performance of both idealized and practical flat-disk shadow shields used to reduce radiant heating between two bodies in a low-temperature vacuum environment. Analytical predictions of shield performance were made for nonuniform radiosity, diffuse surfaces, and generally agreed well with the experimental data for the high-emissivity ($\epsilon \approx 0.9$) and intermediate-emissivity ($\epsilon \approx 0.3$) shields. The experimental shield temperatures, for the low-emissivity ($\epsilon \approx 0.03$) shields tested, tended to be lower than predicted, which was probably due to neglecting the directionally-dependent, nondiffuse properties of the shield material.

Analytical and experimental results demonstrated that: (1) the heat transfer through a shadow-shield system can be decreased by increasing the number of shields and/or spacing of shields and by decreasing the emissivity, (2) decreasing the lateral conductance of a shield increases the radial temperature gradient across the shield as well as the heat transfer, and (3) the use of high-emissivity coatings on annular rings of shields provides an effective method of altering shield temperature profiles.

A lightweight shield concept was evolved that consisted basically of a circumferential ring with shield material stretched and secured to one or both sides of the ring (single- or double-sheeted). The double-sheeted shields significantly outperformed the single-sheeted shields and appear to be a practical concept for lightweight-shield design.

Experimental data were also obtained on the performance of tubular structure members for shield support and gave fair agreement with analytical predictions. These tests demonstrated that the selective placement of high-emissivity coatings on the external surfaces can significantly reduce the strut heat transfer.

Finally, an integrated system for a hypothetical space vehicle and mission was designed, scaled down, and tested to examine the interaction between shields and their necessary supports. Shield-support interactions were determined for systems with the shields pinned in place, welded in place, and welded in place with the shields and struts selectively coated. Although no analysis was made of the shield-support interactions, it was determined that separate analysis of the shields and supports could be extremely helpful in determining how and where the shields should be connected to the support members.

INTRODUCTION

Thermal radiation barriers provide an effective means of limiting the radiant heat transfer between bodies in a vacuum. Because the environment of space provides a good vacuum, radiation barriers can be used as a method of thermal protection for many space vehicle applications. Two forms of radiation barriers of recent interest are multilayer insulation and shadow shields. Multilayer insulation (e. g. , refs. 1 and 2) consists of closely spaced radiation barriers separated by low-conducting spacers and provides one of the most efficient vacuum insulations currently available. Shadow shields are also radiation barriers, but are spaced farther apart to allow more of the heat to escape to the surrounding low-temperature space environment. As a result, shadow shields can provide performance superior to that of an equal number of closely spaced shields. Considerable analytical and experimental effort has been devoted to the application of multilayer insulation to space vehicle systems (e. g. , refs. 3 to 5) while little has been devoted to the problems of shadow-shield applications. Some recent studies in the area of thermal protection for solar probes (e. g. , refs. 6 and 7) and for cryogenic propellant tanks (e. g. , ref. 3) have indicated that weight penalties for thermal protection systems can be reduced substantially with the use of shadow shields.

Shadow shields, in general, are best applied where the major radiant heat load is unidirectional such as on long-duration interplanetary missions where the spacecraft is sun oriented. For solar probe missions, the shields can be used to reduce the intense payload heating during near passes to the sun. On vehicles where cryogenic propellants must be protected from both the warmer payload and solar heating, the vehicle axis can be oriented along a sun vector with the payload to the sun and the shields placed between the payload and the cryogenic tank. The sun-orientation requirement does not appear to be a detriment since most lunar and planetary spacecraft to date have utilized sun orientation. In Earth orbital missions or missions in the near vicinity of other planets, however, fixed shadow-shield systems cannot effectively afford thermal protection from both the sun and planets and, hence, must be augmented or possibly replaced by other protection systems (e. g. , multilayer insulation).

Shadow shields with varying shapes have been analytically investigated (refs. 8 to 12) including flat plates, spheres, hemispheres, cones, etc. , and combinations thereof. Some experimental work has been done on the use of a single flat shield for temperature control of a conical payload (ref. 13) and on the heat transfer between two flat surfaces and a flat and hemispherical surface (ref. 14). The work presented herein[1] investigates the thermal characteristics of multiple flat shadow shields - both ideal and practical - used to reduce the heating between a heat source and heat sink. One advantage of the flat

---

[1]A preliminary report of this work was given in ref. 15.

shields is that they will take up little space on a space vehicle which makes them amenable to use between vehicle components (e.g., mounted between a cryogenic tank and a payload). The experimental program was undertaken to: (1) examine the effects of the pertinent variables on shadow shield performance; (2) determine the adequacy of previously existing analyses for predicting shield performance (e.g., ref. 8, which assumes diffuse, uniform radiosity surfaces) as well as that of a more detailed analysis developed concurrently with this experimental program which assumes diffuse, nonuniform radiosity surfaces (complete analysis is presented in ref. 16); and (3) provide some insight as to how an integrated shadow-shield system might be designed and the inherent problems involved.

Experimental data were obtained to determine the effect of shield spacing, number of shields, surface properties, lateral conduction, and targeting (use of high-emissivity annular rings) on the overall performance of basic shield systems. Data were also obtained on thin, lightweight shadow shields designed for practical application to a realistic system and on tubular structural members that were representative of shield supports. Finally, a scale model of a shadow-shield system was designed, fabricated, and tested to examine the performance of an integrated system and to probe into some of the practical problems of shield application.

EXPERIMENTAL APPARATUS

Basic Experimental Hardware

The experimental apparatus consisted basically of a heat source and a heat sink between which various shadow-shield configurations were suspended. The apparatus shown in figure 1 was designed such that the primary mode of heat transfer into the heat sink was via radiation from the heat source through the shadow-shield system being tested. This was accomplished by: (1) performing the experiments in a vacuum chamber with liquid-nitrogen cold walls in order to minimize gaseous conduction and environmental radiation and (2) by providing low conductance paths between the heat sink and the warmer, external environment.

The heat source consisted of a 1-inch thick copper disk, 12.75 inches (32.4 cm) in diameter, with calrod heaters brazed to the lower surface. An automatic control device maintained its temperature to within $\pm 1^O$ R (± 0.56 K) of its set point. The upper surface of the copper disk was coated with a high-emissivity, high-temperature paint whose thermal properties were predictable to a temperature of 810° R (450 K). The copper disk was mounted to a stainless steel support plate by eight 0.25-inch- (0.635-cm-) diameter, 3-inch- (7.62-cm-) long stainless steel support rods. Support of the heater was provided

by low-conducting cable attached from the steel plate to the heater-shield support structure surrounding the liquid-nitrogen tank.

The support structure shown was used both to suspend the heater and shadow shields and to provide a means of adjusting the spacing between shields and heater. Spacings could be adjusted to give heater-to-tank distances of 0 to 12 inches (30.5 cm). The shields were also suspended by low-conducting cables, and in some cases by fine locket chain, in order to reduce shield conduction losses to less than 0.01 Btu per hour (0.0029 W).

The flat-bottomed liquid-nitrogen (LN_2) tank shown served as the heat sink. The rate of heat transferred into the tank was determined by metering the boiled off N_2 gas. The tank's cylindrical sidewalls and flat bottom were made of copper in order to minimize any temperature gradients within the tank. The tank bottom was 12.75 inches (32.4 cm) in diameter and was coated with a high-absorptivity paint ($\alpha = 0.86$), and its sides were insulated with multilayer insulation to minimize stray radiation heat leaks. The tank lid was made of stainless steel and was suspended from the horizontal channel sections by four stainless steel rods. The lid contained a fill and vent line plus a dip tube to assist in emptying the tank upon completion of an experimental run. In order to minimize conductive heat leaks into the LN_2 tank, the horizontal channel sections which supported the entire apparatus were cooled with LN_2. These channel sections were mounted to the vacuum chamber door as shown in figure 2. Also mounted on this channel were two circular liquid-nitrogen shrouds coated with a high-absorptivity paint ($\alpha = 0.86$). The vacuum chamber contained a cylindrical coated LN_2 shroud so that, when the door was mounted to the chamber, the entire experimental apparatus was surrounded by a relatively cold (140° R or 77.8 K) highly absorptive environment at a pressure of 10^{-6} to 10^{-7} torr.

It should be noted that the LN_2 tank shown in figure 2 has an ellipsoidal bottom. This particular tank was made of aluminum and was used in some of the tests in order to more closely simulate the shape of a realistic tank. Also shown in figure 2 are the various access ports on the door containing the LN_2 coolant lines, the LN_2 tank fill and vent lines, power leads and thermocouple leads, and the crank mechanism used to raise and lower the shields and heater. Not shown is an observation port located in the cylindrical vacuum chamber in which the experiment could be visually observed. The cylindrical LN_2 shroud within the chamber contained a hinged flap that could be opened during observations and closed during testing to eliminate radiation from this room temperature observation port.

Shadow Shields

Several types of shadow shields were used throughout the test program and are sum-

4

marized in table I. All shields were 12.75 inches (32.4 cm) in diameter and most had four attachment points for securing support cables or chains. Various shield materials and thicknesses were used to provide a range of shield surface properties and lateral conductances. Figure 3 shows a shield that is representative of the relatively thick, copper, stainless steel, and aluminum shields used (shields I to IV of table I). A thinner (0.015-in. (0.0381-cm)) stainless-steel shield is shown in figure 4 (shield V of table I). The ridges were required to stiffen the shield to avoid sagging when supported from its attachment points. Figure 5 shows the method of construction used for low-conducting Mylar shields (shield VI of table I) and the laminated aluminum-Mylar-aluminum (AMA) shields (shields VII and VIII). It consisted basically of a circumferential ring with the shield material stretched across and cemented to the ring. This particular shield (fig. 5) has been "targeted," that is, it has a high-emissivity band on its outer radius.

A similarly constructed shield (shield IX) using an "O" ring for support and double-aluminized-Mylar for shield material is shown in figure 6. This is a scale model of a shield that is representative of what might be used in a typical space-vehicle application. The tabs shown were used for attachment to support members. The remaining shields of table I (X to XII), the double-sheeted shields, are constructed identically but with an additional sheet of aluminized Mylar cemented to the other side, hence completely enclosing the ring.

Integrated Shield System

The test program also briefly investigated heat transfer through tubular support members for shadow shields and the combined effects of shields and shield supports. Figure 7 gives the physical characteristics and instrumentation locations for the test specimens used in the support heat leak tests.

Figure 8 shows a scale model of a shadow-shield system with shields and their necessary supports mounted on the end of the ellipsoidal-bottomed tank ($\sqrt{2}$ ellipse). Additional details of the shield system are given in figure 9. The arrangement of the structural supports for the model were influenced by experimental considerations. For example, pairs of structural members terminate on a common copper pad which is, in turn, compressed against the nitrogen tank by a circumferential stainless steel hose clamp. The stainless steel tubes are brazed to the copper pad on the tank end and are brazed to a copper plate (simulated payload) on the other end. This arrangement facilitated easy removal of the shield system to change shields or make other alterations. Initial tests with the system used stainless steel pins to hold the shields in position while in later tests the shield support tabs were spot welded within the cage structure.

The ellipsoidal tank surface was also coated with a high-absorptivity paint. The same paint was used on the flat-bottomed tank and on the LN_2 shroud of the chamber. The simulated payload was coated on both sides with the same high-temperature paint used on the heater. It was maintained at a given temperature by the heater which was located 1 inch (2.54 cm) below it during testing.

Instrumentation

Instrumentation was provided for measuring shield temperatures, temperatures at various locations on the test facility, vaporization rate from the nitrogen tanks, pressure of the nitrogen tank, and pressure level of the vacuum chamber.

The shadow-shield temperatures were obtained with iron-constantan and copper-constantan thermocouples, the latter being used for the lower temperature measurements. Figure 3 shows a typical application of thermocouples for the thicker high-conducting shields (shields I to V in table I). Thirty-gage (0.01-in. - (0.0254-cm-) diam) thermocouples were used and spotted at various intervals across the shield radius. The thermocoupling technique used on the thinner low-conducting shields is demonstrated in figure 10 (shields VI to XII). Forty-gage (0.003-in. - (0.00762-cm-) diam) thermocouple wires were used with their leads laid along isotherms for some distance before leaving the shield to eliminate any influence of the lead wires on the local-shield temperature. Aluminized-Mylar patches were placed over the thermocouples on the aluminized-Mylar shields because the cement used to affix the thermocouples had a high absorptivity and could locally influence the temperature of the low-conductance shields.

The structural members as described in figure 7 were also thermocoupled with 0.010-inch (0.0254-cm) wire. The support system for the scale-model system used 0.003-inch- (0.00762-cm-) diameter wire for the thermocouples (see fig. 11). A smaller diameter wire was used initially (0.001 in. (0.00254 cm)) but caused considerable difficulty and was abandoned for the larger and somewhat more rugged 0.003-inch (0.00762-cm) wire.

The various test facility temperatures measured included those of the heater, liquid-nitrogen tank, liquid-nitrogen shroud, tank fill and vent lines, tank supports, and the cage structure surrounding the liquid-nitrogen tank.

The overall accuracies of all temperature measurements were, in general, on the order of $\pm 5^O$ R (3 K) with the exception of those on the low conductance, double-aluminized Mylar shields (shields IX to XII). On these shields, it was estimated that the thermocouple installation technique resulted in temperatures that were only accurate to within ± 5 percent of the undisturbed shield temperature.

The vaporization rate (boiloff) from the liquid-nitrogen tank, which was used to deter-

mine the heat transfer rate, was metered by either of two wet test meters having over-lapping ranges varying from 0.01 to 1.5 cubic feet per minute (4.7×10^{-6} to 707×10^{-6} m^3/sec). Their overall accuracies were approximately ±1 percent.

The tank pressure, which was measured by a mercury manometer, was isolated from atmospheric pressure variations by a constant back-pressure device similar to that described in reference 17. This device was not used for the higher boiloff rates (>0.3 ft^3/min or 140×10^{-6} m^3/sec) where the equilibrium boiloff rate could be obtained in a short-time period.

PROCEDURE

In a typical experimental run, the apparatus was cold soaked for 4 to 5 hours to insure that all the lines and support rods leading to the LN_2 tank were near the LN_2 design temperature. Then power was applied to the heater to maintain it at a given temperature level until the boiloff rate and all shield temperatures stabilized. The boiloff gas from the LN_2 tank passed through a constant back-pressure device into a water-saturation pot and then through the wet test meter. The boiloff gas volume flow rate along with the gas temperature and pressure as well as the LN_2 tank pressure were used to determine the heat transfer rate into the LN_2 tank. This heat transfer rate less the calculated miscellaneous heat leaks (about 1 to 2 Btu/hr or 0.29 to 0.58 W) represented the net radiant heat transfer rate into the bottom of the LN_2 tank. The miscellaneous heat leaks included conduction through the fill and vent lines, tank support rods, the dip tube, and radiation and reflections from the surrounding liquid-nitrogen shroud.

Subsequent data points were obtained by changing the heater temperature or by varying the spacing between the shields. New spacings were observed through the observation port with the assistance of a scale mounted on the heater support plate (the scale is shown in fig. 1). Heater temperatures of 520°, 650°, and 800° R (289, 361, and 444 K) were used. The majority of the data were taken at the higher temperatures to drive the heat transfer rate up into a measurable range for the low heat flux shield configurations.

RESULTS AND DISCUSSION

General Approach

In order to establish grossly what influences the heat transfer rate through a set of N (see appendix A for a definition of all symbols) shadow shields, consider first the simple case of the heat transferred between two surfaces separated by N infinite parallel

plates. From reference 8, for grey, diffuse surfaces with equal emissivities, the heat transfer between a warm surface H and a cold surface T is given by:

$$\frac{\dot{Q}}{A} = \frac{\sigma\epsilon\left(T_H^4 - T_T^4\right)}{(2 - \epsilon)(N + 1)} \tag{1}$$

From this equation, it is apparent that the heat transfer rate can be reduced by decreasing the emissivity and/or increasing the number of shields.

The assumption of infinite parallel plates dictates that all the heat leaving a shield surface will be intercepted by the adjacent surface. When finite shields are spaced some distance apart (i. e. , shadow shields), only a fraction of the heat leaving a surface strikes the adjacent surface. The remainder escapes to the low-temperature environment of space from the edge of the shadow shield array. The effect of spacing is not included in the simplified equation presented, but increasing the spacing decreases the heat transfer rate. Also, for some configurations, the shield lateral conductance becomes important. By increasing the conductance across the shield radius, heat can be conducted out to the edge of the shield array where it can be radiated from the system.

The preceding discussion indicates that the heat transfer rate can be reduced by decreasing the emissivities and increasing the shield number, spacing, and lateral conductance. The experimental program was designed to investigate the influence of these variables as well as some of the effects of realistically applying the shields. The experimental program was organized and is reported in the following manner: (1) determination of the emissivities of the basic experimental apparatus and the shield surfaces used (Emissivities of Experimental Surfaces); (2) determination of the effect of shield spacing, number, emissivity, and lateral conductance on the performance of somewhat idealized shields (Basic Shield Tests); (3) examination of the performance of practical lightweight shadow shields independent of their required support structure (Practical Shield Tests); (4) investigation of the heat transfer through typical shield support members independent of the shields (Structural Heat Leak Tests); and (5) determination of the performance of an integrated shadow-shield system and the interaction between the structural support members and the shields (Performance of Scale Model).

Wherever possible, the experimental results were compared with existing analyses. The analyses used are taken from reference 16 and, for convenience, are briefly described in appendix B for both shadow shields and tubular struts. The work described in reference 16 considered three analytical models of varying complexity for shadow shields: (1) diffuse surfaces with uniform radiosity[2] (simplified-diffuse), (2) diffuse surfaces with

---

[2]Radiosity is the rate at which radiant energy leaves a surface. It is the sum of the radiant energy emitted from the surface and the incoming radiant energy that is reflected from the surface.

radiosity as a function of position on the shield or nonuniform radiosity (exact-diffuse), and (3) surfaces that emit diffusely and reflect specularly with uniform radiosity. In general, the exact-diffuse analysis was used throughout this report for comparing the experimental data even though some of the lower-emittance shields had properties that were highly specular and directionally dependent. Occasional comparisons are made to point out the differences between the various analyses and their areas of applicability.

Both heat transfer rates and/or shield temperatures were used to compare analytical and experimental results. Many of the basic shield configurations tested were purposely designed to give relatively high heating rates in order to maintain reasonable experimental accuracies on heat transfer rates. This is why the heater, simulated payload, tank, and, occasionally, the shields were coated with high-emissivity paints. For the scale-model tests where realistic configurations and surface properties were used, the heat transfer rates were too low for measurement and temperature data were relied upon for any comparisons with the analytical results.

Emissivities of Experimental Surfaces

The emissivity of the high-temperature paint used on the heater, simulated payload, and on some shields was dependent on temperature and is shown in figure 12. All the data points above 500° R (278 K) were determined in an emissometer as described in reference 18 and have a probable error[3] of ±5 percent at room temperature and ±3 percent at the higher temperatures. The lone point at 140° R (77. 8 K) was determined with the experimental apparatus by coating both the heater and the flat-bottomed LN_2 tank with the high-temperature paint and measuring the heat transfer rate between the two for various heater temperatures (520° to 800° R or 289 to 444 K). The heater was spaced 0. 5 inch (1. 27 cm) from the tank (L/R_o = 0. 0784). With the heater emissivity known, the heat-transfer equations were solved for tank absorptivity. The absorptivity of the paint at 140° R (77. 8 K) was found to be independent of heater temperature within the experimental accuracies of the system and thus it was assumed that the absorptivity and emissivity were equal. The error involved in determining the emissivity at 140° R (77. 8 K) was on the order of ±5 percent due to the accumulation of errors involved in measuring the heat transfer rate (determined from boiloff rate), heater temperature, and heater emissivity. The line drawn through the data represents a least squares curve fit for a second-degree polynomial and should predict the actual emissivity to within ±5 percent.

---

[3]The term "probable error" is not used in its strict mathematical sense in this report, that is, it is not 0. 675 times the standard deviation. It represents the best estimate of the errors involved in determining a given quantity.

The coating used on the LN_2 tank and the LN_2 shroud during testing was a paint that is normally used for low-temperature cryogenic applications. Its emissivity, determined by utilizing the facility as described above, was found to be 0.86±5 percent.

Once the emissivities of the heater and tank were known, single-shield tests were performed with the flat-bottomed tank to help determine the emissivities of the noncoated shield materials. In doing this, heat transfer and temperature data were taken with the subject shield suspended midway between the heater and tank (heater-to-tank distance was 0.157 R_o). With the measured heat transfer rate from the experimental apparatus, the heat transfer equations could be solved for shield emissivity. Using this technique and fairing a straight line through the data, the emissivity was determined for the glass-blasted copper shield (shield II) of table I. The measured points were obtained at shield temperatures of 535° and 660° R (297 and 367 K).

In arriving at the emissivities for the AMA material of shields VII and VIII and the double-aluminized Mylar of shields IX to XI, data from the experimental apparatus were used in conjunction with that from other sources as is shown in figure 13. Only one point each was obtained with the experimental apparatus for the AMA and double-aluminized Mylar. The remaining data are for aluminum foil from reference 20 and double-aluminized Mylar from reference 4. Although, not plotted, the straight line function for shield emissivity given in table I for the AMA material, passes through the lone data point of figure 13 and has the same slope as that of the line faired through the data of reference 20.

The parallel lines shown passing through the two double-aluminized Mylar data points were obtained in a similar manner. The upper line (dashed) passes through the lone data point measured by the experimental apparatus of this report. The lower line passes through the data point given by reference 4, which gave the mean value, of total hemispherical emissivity, measured for several clean samples of double-aluminized Mylar. The higher emissivity measured by the experimental apparatus is expected because of possible contamination encountered during fabrication, handling, and instrumentation of the shields. It also should be noted that the total hemispherical emissivity could still be slightly higher than that measured due to the directionally-dependent properties of metallic surfaces. These properties were assumed to be diffuse with the experimental technique used. However, the upper curve (dashed line) was used for most of the analytical results while the lower curve was occasionally used as a lower limit of shield emissivity.

Finally, the emissivity of the stainless steel material, used for the tubular support models, was determined with the emissometer of reference 18. A straight line drawn through the data resulted in the following expressions for emissivity:

$$\epsilon = 0.1618 + 2.03 \times 10^{-4}\, T \quad \text{where} \quad T \text{ is in } ^O R$$

or

$$\epsilon = 0.1618 + 3.65 \times 10^{-4} \, T \quad \text{where} \quad T \text{ is in K}$$

Basic Shield Tests

Shield spacing. - In order to investigate the effects of shield spacing, number, surface properties, lateral conductance, and targeting on the radiant heat transfer, it was desirable to begin with the simplest case and systematically vary one variable at a time. The most readily analyzed case was that with infinitely conducting shields assuming uniform radiosity, which was analyzed previously in reference 8 (a special case of the analysis given in appendix A or ref. 16). This was simulated experimentally with 0.0625-inch- (0.159-cm-) thick copper shields coated with the high-emissivity, high-temperature paint (shield I, table I). The effect of shield spacing on heat transfer rate for a single copper shield centrally located between the heater and flat-bottomed LN_2 tank is shown in figure 14 for various values of heater temperature. Spacing ratio (L/R_o) is the total distance between the heater and tank divided by tank radius. Due to accumulation of random experimental errors (i.e., surface properties and temperature and boiloff measurements), the probable error in the data is on the order of ±7.5 percent. Since the total uncertainty depends upon the number of shields and their spacing ratio, the errors for several representative shield configurations are given in table II.

The analytical results in figure 14 represent both the simplified-diffuse and exact-diffuse analysis since the radiosity is essentially uniform (reflected term in the radiosity is relatively small). From the figure, it is apparent that increasing the spacing ratio between components decreases the heat transfer rate and that the general agreement between the analysis and experimental data is good.

Number of shields. - The effect of shield number as well as spacing ratio is shown in figure 15 for a heater temperature of 800° R (444 K). The heat transfer rate is given for zero, one, three, and five shields located between the heater and the LN_2 tank (the five-shield configuration was depicted in fig. 1). Again, the agreement between data and analysis is quite good. It is apparent that the shields provide an effective method of reducing radiant heat transfer. For example, at a spacing ratio of 0.1, a single shield placed between the tank and heater reduces the heat transfer by nearly a factor of 2. With three shields, the rate is reduced by about a factor of 4 even though the individual spacings between the shields have decreased. Furthermore, the relative advantages of shadow shields is minimized here because of the high emissivity surfaces used. More practical applications would use lower emissivity shields. Also, no attempt was made to optimize the relative spacing between shields for a given shield number; that is, all data

were given for equally spaced shields. Depending on the particular configuration used, the heat transfer rate can further be reduced by using nonequal intermediate spacing between shields (see ref. 16).

The average shield temperatures for the shield configurations discussed in the previous two figures are shown in figure 16. It should be noted that the temperature gradients across the individual shields only varied from 2^O to 4° R (1.1 to 2.2 K) from the center of the shields to the outer edges. For purposes of this figure, an average temperature was plotted, and it is seen that it generally agrees with the analytical predictions to within ±2 percent.

Shield emissivity. - Although heat transfer rates can be reduced by increasing the spacing ratio and/or the number of shields, major reductions in heat transfer rates are best realized by using lower emissivity surfaces. This is demonstrated in figure 17 where the heat transfer rates of both high emissivity ($\epsilon \approx 0.94$) and intermediate emissivity ($\epsilon \approx 0.26$) glass-blasted copper shields (shields I and II, respectively, of table I) are shown as a function of shield spacing ratio and number. Data are given for one- and three-shield configurations. It is apparent that emissivity has a strong effect on the heat transfer rates. For example, at a spacing of 0.314, the heat transfer rate for one shield is reduced by a factor of about 3.5 by going from a shield emissivity of 0.94 to 0.26. For a three-shield configuration, where more lower-emissivity surfaces are present, the corresponding change in emissivity results in a factor of 8.5 in heat transfer rates. So the use of lower emissivity surfaces gives a more pronounced effect of shield number as evidenced by the displacement of the curves. Also the slopes of the curves indicate that spacing ratio has a stronger effect as emissivity is decreased for multiple shield systems. The efficiency of shadow shields become more evident when it is realized that surfaces with emissivities an order of magnitude less than that of the copper are commonly obtainable (e.g., aluminum or gold films as discussed in ref. 4).

The analytical results for this figure are given for both the exact-diffuse and the simplified-diffuse analysis. It should be noted that the glass-blasted surfaces of the copper shield appeared highly diffuse. For the high-emissivity shields and the single glass-blasted copper shield, the analytical results of the two analyses are within 1 percent of each other and the differences are not distinguishable on the figure. Differences are noted, though, for the lower emissivity three-shield configuration. The simplified-diffuse analysis underestimates the heat transfer rate and tends to be more in error for the larger spacings. The results of the two analyses approach each other at the lower spacings where the radiosity becomes more uniform (radiosity is uniform for infinite parallel plates). Actually, the results will also converge at the higher spacings (not shown) where the reflected term in the radiosity becomes small (ref. 16). The differences between the two analyses depend upon both the relative spacing and emissivity; but, in general, the simplified diffuse analysis can seriously underestimate the heat transfer

rate for low-emissivity shields with spacing ratios on the order of 0.1 between individual surfaces. For example, if the three shields in figure 17 had an emissivity of 0.03 and an overall spacing (L/R_O) of 0.314, the assumption of uniform radiosity would give heat transfer rates a factor of 65 lower than the nonuniform radiosity results.

The shield temperatures for the glass-blasted copper shield tests are shown in figure 18 as a function of spacing ratio for both one and three shields. The results from the exact-diffuse and simplified-diffuse analyses are shown. There are no detectable differences for the single shields. The shield temperatures were measured on the shield edges only to avoid disturbing the clean surfaces. As a result the experimental temperatures shown are slightly lower than the mean temperatures of the shields. For the high-temperature closely-spaced shields, there is about a 4° R (2.2 K) radial temperature drop across the shield. The widely-spaced lower-temperature shields have radial temperature drops on the order of 1^O R (0.55 K). This will tend to shift the data more toward the analytical exact-diffuse results. Although the results are not conclusive, it appears that the exact-diffuse model more nearly predicts the experimental results especially for the lower-temperature shield where the shield radial temperature gradients would be at a minimum.

Shield lateral conductance. - The experimental results discussed thus far used thick copper shields in order to insure relatively uniform temperatures across the shield radius. Since thick copper shields are impractical for most applications, due to weight considerations, it is desirable to examine the effect of using thinner, lighter materials.

The analytical[4] and experimental radial temperature profiles of five separate shields with varying shield materials and thicknesses are shown in figure 19 for a spacing ratio of 0.314. All shields were coated with the high-temperature paint in order to establish a common emissivity and thus isolate the effect of shield lateral conductance (kt/R_O^2) on both the temperature profiles and the heat transfer rates. The radius ratio (R/R_O) on the abscissa gives the position across the shield radius. In figure 19(a), the experimental temperature profiles of two high-lateral-conductance shields are compared with the calculated temperature of an infinite conductance shield. The data for the high-conducting copper shield (shield I), used in most of the previous figures, indicate only a 4° R (2.2 K) drop in temperature across the entire shield while that for the aluminum shield (shield III) gives a 7° R (3.9 K) drop. Figure 19(b) gives both the experimental and analytical profiles for the intermediate conductance stainless-steel shields. As indicated by the figure, lowering the lateral conductance causes higher temperatures near the center of the shield and lower temperatures near the edge of the shield. This is further demonstrated in figure 19(c) for the low-conductance Mylar shield where the edge temperatures drop off sharply. The analytical results shown are for both the Mylar shield and for a shield with

---

[4]Exact-diffuse analysis is used throughout the remainder of this report.

zero lateral conductance. The temperature of the shield center is higher than the edge because the view factors from the heater to an elemental area in the center of the shield are higher than the view factor from the heater to a corresponding elemental area near the shield edge.

Comparing the analytical heat transfer rates indicates that decreasing the lateral conductance causes a slight increase in heat transfer rates. This is obvious since the higher conductance shields can conduct heat from the center of the shield to the edge where it can be radiated to space easier. The effect of lateral conductance is, in general, confirmed by the experimental heat transfer rates with the exception of one of the higher conducting shield tests. The discrepancy is well within the probable experimental error, though, which is on the order of ± 7.5 percent for this configuration. Although it is not demonstrated experimentally, the lateral conductance parameter and the spacing ratio provide the information necessary for thermal scaling. For given boundary temperatures and surface properties, the thermal performance will be identical for any size system as long as the relative shield spacing ratio (L/R_O) and the lateral conductance (kt/R_O^2) are held constant.

The radial temperature gradients across low-conductance shields also depend upon the relative spacing between the shields as well as the number of shields. This is demonstrated in figure 20 where the temperature profiles of three high-emissivity, low-conductance shields are shown for various spacing ratios. Also noted on the figure are the temperature levels for infinite-conductance shields. The shield temperatures for the close spacing ratio $(L/R_O = 0.314)$ are seen to drop off sharply near the shield edge. As the spacing is increased, the temperature profiles become more gradual or flatter. In the extremes, as the spacing ratio approaches either zero or some large value, the shield-temperature profiles will become flat since all parts of the shield will be exposed to a constant radiant heat flux. It is interesting to note that the edge temperature of the low-conducting shields for the spacing ratios shown can drop to a level lower than the center of the adjacent colder shields. Again the agreement between the data and the analysis is good.

The analytical and experimental heat transfer rates are also given for each spacing along with the ratio of heat fluxes for zero- and infinite-k shields. The data indicate that the low-conducting shields have heat transfer rates about 10 to 30 percent higher than that for the high-conducting shields. This difference is a function of shield emissivity as well as the shield number and spacing. For example with a shield emissivity of 0.03, and the same three-shield configuration given in figure 20(a), the exact-diffuse analysis indicates that the heat transfer rate for zero-conductance shields will be about 1.5 times higher than that for the infinite conductance shields. So the emissivity has a strong effect on the difference. Again, in the extremes, as the spacing ratio approaches zero or some large value, the results for the low- and high-conducting shields will converge.

14

Shield targeting. - Since space vehicle weight considerations will probably dictate the use of thin shields or low-conductance shields, the temperature profiles across the shields must be considered in the system design. For some applications, it may be of interest to tailor the shield-temperature profile to meet some design constraint. This can be accomplished by selectively coating various annular areas on the shield or shields (shield targeting). An example of shield targeting is given in figure 21 where the shield-temperature profiles of a two-shield configuration are plotted for three different spacings. The shield nearest the LN_2 tank is a low-conducting Mylar shield (shield VI) coated on both sides with the high-temperature paint. The other shield is an aluminum-Mylar-aluminum (AMA) laminated shield (shield VIII) that is completely coated on the heater side and has a 1-inch (2.54-cm) band of high-temperature paint on the edge of the other side (e.g., see fig. 5). The arrangement of the shield spacings in this test is different than previously used in that the shield nearest the LN_2 tank has a fixed intermediate spacing ratio (s/R_o) of 0.157 while the targeted shield is evenly spaced between this shield and the heater. The colder shield spacing was fixed to reduce the number of variables. As is evident from the figure, the temperature profiles can be altered considerably with the use of the targeting concept. Without targeting, the temperatures would be warmest in the center and decrease monotonically outward as shown in the previous figures. For the closer spacing ratio $(L/R_o = 0.314)$, the targeted band on the warmer shield causes the edge temperature of the colder shield to increase sharply above that of its center. The center remains relatively cool because of the low view factors between the targeted edge of one shield and the center of the other. As the spacing is initially increased, these view factors increase and, hence, proportionally radiate more heat to the center of the colder shield. Then at some point the view factor begins to decrease due to the increased spacings involved. For the largest spacing used, the colder shield temperature profile is nearly flat. The solid lines again represent the exact-diffuse analysis and appear to predict the performance reasonably well. The disagreement noted may be due to inaccurate knowledge of the surface properties of the AMA material. The method of determining the emissivity assumed diffuse surface properties as does the analysis used. Real surfaces, such as the AMA material used, have properties that are directionally dependent. For example, the directional emittance of metallic surfaces tends to be lower at angles near the surface normal and higher at the larger angles from the normal (see ref. 19). This could cause lower temperatures at the center of the colder shield. The particular targeted system used here has little practical value and was intended primarily to demonstrate the concept of targeting and to determine whether the results could be predicted. In a more realistic application, the shield-temperature profiles might be altered for thermal-stress considerations or to help make the shadow shield thermally compatible with their necessary support structure for an integrated system.

Practical Shield Tests

Single-sheeted shields. - The somewhat idealized shields used thus far have been designed primarily to help determine the effect of certain variables on shadow-shield performance and as a result are not generally suitable for realistic applications. In general, shields designed for space vehicle applications should be lightweight, rugged, and have low-emissivity surfaces. One method of shield construction that may fulfill these requirements consists of lightweight shield material attached to a circumferential support ring. This type of construction was demonstrated for the experimental shield shown in figure 6 (see table I, shield IX for details). The tabs on the support ring were required for subsequent testing of this shield and are not necessarily representative of a vehicle application. The shield material was stretched taunt and cemented to the ring. Application of this general concept for a space-vehicle system would, of course, require a rugged shield material. A possible material could consist of a fiberglass mesh bonded between two layers of aluminum or between two layers of Mylar that are aluminized on the exposed surfaces. The fiberglass mesh would serve as a reinforcing material and would also prevent holes or tears in the material from propagating. In any event, the shield would approach a zero-conductance shield which is adequately simulated by the 1/4-mil (0.000635-cm) double-aluminized Mylar used for the experimental shield.

The low-emissivity, low-conductance surfaces presented some temperature instrumentation problems as demonstrated in figure 22. The shield-temperature profiles are shown for a single double-aluminized Mylar shield (shield IX) using two separate methods of thermocoupling: (1) thermocouples cemented to the shield surface along various isotherms and (2) the same shield with 0.5 by 1.5 inch (1.3 by 3.8 cm) double-aluminized Mylar patches cemented over the thermocouple junction and the last inch of lead wires. These patches are visible in the photograph shown in figure 10 and were required because the cement used to secure the thermocouple to the shield had a high emissivity and locally affected the temperature of the low-conducting, low-emissivity shields. The analytical results shown on figure 22 demonstrate that, for a single shield, the temperatures are very insensitive to shield emissivity. Therefore, the results shown closely represent the true temperature of the shield especially on the inner portions of the shield. The data shown are for thermocouples located on the shield surface facing the LN_2 tank. Similar tests, not shown, on an AMA shield (shield VII) with the thermocoupled surface facing the heater gave temperature readings 3 to 7 percent higher than the analytical results (nonpatched thermocouples). For the double-aluminized Mylar data shown, the nonpatched temperatures are 7 to 10 percent low while the patched temperatures are generally 5 percent low and have less scatter. Therefore, it is felt that the temperature measurements made on the double-aluminized Mylar surfaces are only good to within ±5 percent.

The shield-rim temperatures are roughly 200° R (111 K) lower than the center of the shield. This is primarily caused by the relatively high-emissivity stainless-steel ring that supports the shield material. The ring surface exposed to the warmer heater is covered with the low-emissivity shield material while the remainder of the surface (about 3/4 of the ring surface area) is exposed to the colder environment and has an emissivity of about 0.25. This reduces the heat absorbed by the ring from the heater and increases the amount of heat emitted over 3/4 of the ring surface area. The experimental data is simulated analytically by assuming the side of the shield facing the LN_2 tank has a targeted band that has an emissivity of 0.25 and a width equivalent to 3/4 of the ring circumference. As a result, the shield-rim temperature drops considerably below that for a shield with uniform emissivity which is on the order of 600° R or 333 K for this particular configuration. It is apparent that the analysis predicts the edge temperatures reasonably well.

Double-sheeted shields. - For the type of shield construction used, a logical step toward increasing the shield efficiency is to add an additional sheet of shield material to the open side of the ring, hence forming a double-sheeted shield (fig. 10). The additional weight for the extra sheet of material would be negligible since the major portion of the shield weight would be due to the circumferential ring. The temperature profiles and heat transfer rates are shown in figure 23 for a double-sheeted shield where: (a) all surfaces have the emissivity of the double-aluminized Mylar; (b) all surfaces are coated with the high-emissivity, high-temperature paint; and (c) only the external surfaces are coated with the high-temperature paint.

Two separate methods of analytically simulating the double-sheeted shield were investigated. The first method, represented by the solid lines, used two flat shields with a near-zero spacing and targeted edges to simulate the double-sheeted shield and its support ring. By assuming a near-zero spacing, little energy is allowed to escape to the environment from between the shields. This is a reasonable assumption since, in reality, all the radiated and reflected energy from within the sheets is intercepted by the surrounding support ring and, hence, is not allowed to escape directly to the environment. The analytical intermediate spacing ratios (s/R_o) used between the surfaces, starting from the heater were 0.157, 0.0001, and 0.157 whereas the actual intermediate spacings between the surfaces were 0.147, 0.02, and 0.147. The colder side of the warmest sheet had an area-weighted, targeted band equivalent to the product of the ring emissivity and its exposed-surface area. For the colder sheet, it was assumed that the area cemented to the ring had an absorptivity and emissivity of 1. (No targeting was used for the shield in fig. 23(b) since all surfaces were coated with the H. T. P.)

The second method represented by the dashed lines used the actual intermediate spacing ratios of the shields (0.147, 0.02, 0.147) and assumed the edges of the shields were closed off by a cylindrical side whose height was the same as the support-ring di-

ameter. The emissivity and absorptivity of the side piece between the shields was assumed to be that of stainless steel.

The experimental heat transfer rate for the double-sheeted shield in figure 23(a) is about 5.2 Btu per hour per square foot (16.3 W/m^2) which is about 40 percent less than that for a single shield tested under the same conditions. The extra sheet of material reduced the heat transfer rate significantly with only a minor increase in shield weight. The analytical heat transfer rates for the double-sheeted shields are lower than the experimental rates despite the higher analytical temperatures. It is felt that this was primarily due to ignoring (analytically) the radiation and reflections from the experimental surroundings (e.g., LN_2 shroud) which start to become significant at the lower heat flux levels. Because of the inaccuracies at these low heat flux levels, it is best to (1) only make relative comparisons between experimental heat fluxes and (2) compare shield temperatures which are less sensitive to these errors because shield temperature is primarily determined by the higher energy levels from the adjacent shield or heater.

The temperature profiles are about the same for both analytical methods and predict the shape of the experimental profile reasonably well. However, there is some disagreement in the temperature level of the colder sheet as well as those temperatures on the shield edge. The discrepancy in the colder sheet temperature could result from (1) inaccuracy of the thermocouple data, (2) variation in shield emissivity, and (3) the directional properties of the shield material (e.g., see refs. 19 and 21). For example, if it is assumed that the inner surfaces of the double-sheeted shield have emissivities 0.004 lower (cleaner surfaces), the analytical results for the warmer sheet would increase by 5° R (2.8 K), while the colder decreased by 12° R (6.7 K). The effect of directional properties (emissivity and reflectivity) is beyond the scope of this report; however, the fact that metallic surfaces emit more strongly at high angles to the surface normal indicates that shield centers will be colder than that calculated by assuming diffuse properties. The discrepancy in shield-edge temperatures is not unreasonable considering that the analytical models assume no physical contact between the edges of the colder and warmer sheets.

The shield used in figure 23(b) was completely coated with the high-temperature paint, both inside and out. The thermocouples did not have patches as the surfaces were painted with a high-emissivity coating. It is apparent that both the experimental temperatures (excluding the rim temperatures) and the heat transfer rate agree well with the predicted results.

The shield used for figure 23(c) was the same as that used for 23(a) only the external (exposed) surfaces were coated with the H. T. P. This particular shield warped severely during testing which undoubtedly affected the experimental results. The experimental temperatures agree reasonably well with the analytical results. However, the heat transfer rates differ considerably but this was probably caused both by (1) the analytical model

not adequately predicting the higher edge temperatures for the colder sheet, and (2) the warpage of the shield which allowed some direct radiation from the heater to the tank.

Comparing the experimental heat transfer rates of figure 23(c) with that of figure 23(a), it is seen that coating the external surface of the double-sheeted shield with the H. T. P. only caused a 150-percent increase in heat flux. For a single-sheeted shield tested under comparable conditions, coating the surfaces with H. T. P. would increase the experimental heat flux from 8.8 Btu per hour per square foot (27.7 W/m^2) to the 220 Btu per hour per square foot (694 W/m^2) level indicated in figure 14, an increase of 2400 percent. The reason that the increase for the double-sheeted shield is so small is that the internal surfaces retain their low emissivities. This could be a beneficial feature of double-sheeted shields for space applications where the meteoroid environment or other environmental factors might cause deterioration of exposed surfaces.

Structural Heat Leak Tests

The experimental tests discussed thus far only considered shields that were thermally isolated from each other from the standpoint of conductive heat transfer. In order to utilize shadow shields on a space vehicle, they must somehow be supported between the heat source and the cryogenic tank. Because tubular structural members provided an efficient, lightweight method of support, their thermal performance was briefly considered for application to an integrated shield system.

The heat transfer rates and normalized-temperature profiles of a tubular member, independent of a shield system, are shown in figure 24 to demonstrate the importance of the external-tube emissivity. Data are given for 12-inch- (30.5-cm-) long stainless-steel tubes (described in fig. 7) that were uncoated and partially coated with the H. T. P. to vary the external-tube emissivity. The tubes were flattened on the ends and bolted to the heater and LN_2 tank. Two low-emissivity shields were suspended between the tank and heater to make the radiant heat transfer from the heater negligible. The shields did not make physical contact with the tubes.

The analytical results were determined with the analysis given in reference 16 (and reproduced in part in appendix B) which assumed diffuse surfaces with temperature-dependent thermal conductivities, internal emissivities, and external emissivities. The analysis did not include radiation from the heater or shields.

The uncoated strut data are for two tubes that have been glass-blasted to provide a uniform-surface finish. The heat transfer rate given is the average rate for a single tube (used two for higher fluxes). The coated strut data are for the same tubes with the outer half of their external surfaces painted with H. T. P. as described in figure 7. By selectively coating the struts, more heat could be radiated to the colder surroundings and

hence reduce the net heat into the LN_2 tank. Although no attempt was made to optimize the coating or its pattern, the results indicate that selective coating of the struts may be helpful for applications where the major portion of heat comes through the struts.

The agreement between the analytical- and experimental-temperature levels as well as the heat transfer rates is not good (fig. 24). However, a relative comparison of the affect of coating shows good agreement between the analytical and experimental temperatures. The measured heat transfer rates were extremely low and were affected by the inaccuracies at these low levels although a decrease in heat transfer rate for the selectively coated strut is definitely apparent. Besides the experimental inaccuracies, it is felt that the assumption of diffuse surfaces for the analytical model caused some of the disagreement shown. Both the directional emittance and nondiffuse reflectance of the stainless steel could cause higher radiant heat transfer rates inside of the tubes.

Similar tests were performed on 6-inch (15.25-cm) struts with the same diameter and wall thickness to determine the effect of strut length and to compare the analytical and experimental results at a level where better accuracies were expected. The results are shown in figure 25 for coated and uncoated struts. Here, the agreement between the analytical and experimental heat transfer rates is better. Comparing the analytical results from figures 24 and 25, it is seen that doubling the strut length reduces the heat transfer rate by a factor of 2.1 for the uncoated struts and a factor of 2.60 for the coated struts. For a purely conducting strut doubling the length should reduce the heat transfer by a factor of 2, so it is seen that the radiation from the struts can have a significant effect on the results. In general, the heat transfer through the tube will decrease with increasing external emissivity and decreasing internal emissivity (ref. 16).

Performance of Scale-Model System

Description of practical shield system. - Now that the performance of both the shields and tubular support members have been considered individually, it is of interest to determine the interactions between the two in a more realistic integrated shadow-shield system. In order to do this and to gain some insight as to the possible problems involved in a realistic system, a preliminary design of a shadow-shield system was made for a hypothetical vehicle and mission and then scaled down and tested. A schematic of the vehicle and its shadow-shield system is shown in figure 26. For simplicity, only the thermal protection of the hydrogen tank was considered.

The vehicle selected was a hydrogen-oxygen upper stage with a 7000-pound- (3170-kg-) propellant load capable of braking a payload into a Mars orbit. Trip time was 200 days during which time the vehicle was sun oriented with the payload toward the sun. The hydrogen tank ($\sqrt{2}$ ellipsoid) and payload diameters were 10 feet (3.05 m). Two

shields were located in the 12-inch (30. 5-cm) gap between the liquid-hydrogen tank and the payload with the first shield 1. 5 inches (3. 81 cm) and the second 10 inches (25. 4 cm) from the hydrogen tank surface. [5] The design concept used for the shields was the same as that discussed previously in the Practical Shield section. The hydrogen tank was assumed to be insulated with 1/2 inch (1. 27 cm) of ground-hold insulation (ref. 3) which could consist of foam insulation with a few external layers of double-aluminized Mylar. The double-aluminized Mylar could afford protection during near planetary operations. The support struts were 1.25 outside diameter by 0.035 inch.(3. 17 o. d. by 0.089 cm) wall titanium tubes, 43 inches (109 cm) long. The titanium tubes were also used for the shield-support rings which were 10 feet (3. 05 m) in diameter. The shield material was assumed to weigh 0. 040 pound per square foot (0. 195 kg/m^2) which is equivalent to the weight of double-aluminized Mylar, 5 mils (0. 0127 cm) thick.

Description of scale model. - A scale model of the shadow shield system was given in figure 8 with additional details of construction given in figures 9 and 11. The scaled-down thermal model used for testing was a result of several compromises to facilitate testing in the environmental chamber. The tank, payload, strut, and shield ring dimensions as well as distance between shields were all linearly scaled down from the full-scale version making radiation exchange between components equivalent. The cross-sectional area of the struts and shield rings were determined primarily by material availability and as a result were not scaled accurately. However, they are generally representative of the relatively low-conductivity metallic structural members. The struts had good thermal bonds on both ends to avoid the analytical problems involved with predicting heat transfer through joints with thermal contact resistance.

The simulated payload was maintained at a given temperature by radiating heat to its lower surface with the heater used in previous tests. The shields used were constructed as discussed previously and were representative of the type shield that might be used for a practical application. The tank used had a $\sqrt{2}$ ellipsoidal surface as did the full-scale version. In order to provide surfaces with known emissivities, both the tank and the simulated payload were coated with the same paints used on the tank and heater in the previous tests. Normally, these surfaces would have low emissivities. Finally, liquid nitrogen, rather than liquid hydrogen, was used for safety reasons. Despite these departures from the full-scale system, the model was sufficient for probing into some of the strut-shield interactions of realistic systems.

Component test. - Before testing the complete scale-model system, several component tests were performed to determine (1) the effect of tank shape on shield perform-

---

[5]A preliminary analysis of the two-shield configuration assuming uniform radiosity (ref. 8) indicated that the radiant heat transfer could be minimized by placing one shield near the payload and the other near the tank.

ance; (2) the adequacy of the flat plate analysis for predicting the performance of multiple, low-emissivity practical shields; and (3) the performance of the scale-model shield configuration independent of the support system. The effect of tank shape on heat transfer rate is shown in figure 27 where data are given for both the flat- and ellipsoidal-bottomed tanks. Also shown are the heat transfer rates for one and three high-conductance shields (shield I) for the ellipsoidal tank. The length L used in the spacing ratio is the distance from the heater to the nearest part of the tank bottom. As a result, the heat transfer rates for the ellipsoidal tank are less than for the flat-bottomed tank because the tank occupies a smaller solid angle as viewed from the heater. The difference in total heat transfer rates is not as large as appears in the figure, however, due to the increased surface area of the ellipsoidal-shaped tank $(1.623 \ \pi R_o^2)$ over that of the flat-bottomed tank (πR_o^2). For the high-emissivity surfaces used, the difference in total heat transfer rate is essentially proportional to the differences in view factors. Again, the analytical results are in good agreement with the experimental heat transfer data.

The effect of tank shape on the temperature profile of a low-conducting shield (shield VI) is shown in figure 28 for both a flat-bottomed and an ellipsoidal-bottomed tank. The data indicate that the temperature profiles are influenced little by the tank shape for the high emissivity surfaces and are readily predicted by the analysis. However, it should be noted that when realistic shield and tank properties (i.e., low emissivity) are used, the shield-temperature profiles can be influenced by tank shape.

With the performance of the high-emissivity surfaces known both analytically and experimentally, the next step was to examine the performance of the more realistic low-emissivity shields for a multishield configuration using the ellipsoidal tank. Figure 29 gives the temperature profiles for a three-shield configuration using a heater temperature of 800° R (444 K). The arrangement of the shields and their intermediate spacings were as shown on the sketch. The shields were single-sheeted, double-aluminized Mylar shields (shield IX). The shield rims were accounted for, analytically, by targeting as described previously in the section on Practical Shield Tests.

Analytical results are given for the actual intermediate spacings (sheet-to-sheet) as well as for smaller intermediate spacings (rim-to-rim). The rim-to-rim spacings are shown as an attempt to account for the radiation that is trapped within the system by the protruding shield rims since the analytical model assumed flat-disk shields. The rim-to-rim spacings should only be used as an estimate of the edge temperature (at $R/R_o = 1$) of the shield. The inner temperatures of the shield are best represented by the actual sheet-to-sheet spacings (solid lines). The experimental results, in general, verify this.

The overall shapes and relative displacements of the analytical temperature profiles are in fair agreement with the experimental data. The general shapes of the profiles are a result of the relative positions of the high-emissivity rims or targeted edges of the shields. The two colder shields have relatively flat profiles because their rims are

facing the adjacent warmer shields as shown on the accompanying sketch. Without the high-emissivity rings, their temperatures would decrease monotonically from the shield centers to the edges. From the figures, its apparent that (1) the analysis reasonably predicts the temperature profiles of the experimental shields and (2) the shield-temperature profiles are very sensitive to the relative location of the higher emissivity rings.

The absolute temperature levels predicted by the analysis do not agree well with the experimental data for several reasons. The biggest discrepancy occurs for the coldest shield and is primarily a result of the radiated and reflected energy from the LN_2 shroud that was not accounted for in the analysis. Rough estimates indicate that this neglected energy could cause about a 20-percent increase in the temperature of the coldest shield (negligible increase for the warmer shields). The other discrepancies noted are the combined results of temperature-measurement errors (±5 percent), possible emissivity variations (e.g., fig. 13), and the diffuse-surface assumptions used in the analysis.

For the vehicle and mission selected, preliminary analysis indicated that only two shields would be required to reduce the radiant heat transfer to an acceptable level. Results of scale-model tests on the selected two-shield configuration, independent of the support system, are shown in figures 30(a) and (b) for both single- and double-sheeted shields (shields IX and X), respectively. The location of the shields with respect to the heater and ellipsoidal tank are identical with those of the scale-model system shown in figure 9. The intermediate spacing ratios given on figure 30 are the spacing ratios used for the analytical results with the total spacing ratio, in each case, being equivalent to the total experimental spacing ratio ($L/R_O = 0.192$).

For the single-sheeted, double-aluminized-Mylar shields used in figure 30(a), the sheet-to-sheet spacings resulted in a calculated cold-shield edge temperature about 50° R (28 K) lower than those measured. If rim-to-rim spacings were used, as discussed for figure 29, the analytical edge temperature would increase to 355° R (197 K). With the exception of the colder-shield edge, the overall agreement between the analytical and experimental temperatures is reasonably good.

The data in figure 30(b) for the two double-sheeted shields shows some discrepancies between the analytical and experimental results. The solid lines are for a near-zero intermediate spacing ratio (0.0001) between adjacent sheets of the double-sheeted shields and the dashed lines are for the actual intermediate spacings with the shield rings being replaced by short cylindrical sides as discussed previously for the double-sheeted shields in figure 23(a). Both analyses overpredict the interior-shield temperatures and give approximately the same results. It is very unlikely that the large differences noted are entirely attributable to errors in measuring temperatures or variation in shield emissivity. For example, if all the shields are assumed to have the lowest emissivities felt possible (lowest line on fig. 13), the temperatures of the shield centers would only drop 1^O, 5°, 9°, and 10° R (0.55, 2.8, 5, and 5.5 K), respectively, for the warmest to the

coldest sheet. On the other hand, a more likely possibility is that the external surfaces of each double-sheeted shield had higher emissivities than the internal surfaces because the inner surfaces were not thermocoupled and did not experience as much handling. However, using the highest and lowest emissivities expected (parallel lines for double-aluminized Mylar on fig. 13), for the external and internal surfaces, respectively, the shield center temperatures would only change $+4^O$, -7°, -2^O, and -15° R ($+2.2$, -3.9, -1.1, and -8.3 K), respectively, for the warmest to the coldest sheet.

These variations in shield emissivity obviously cannot account for the differences shown. Also, if the radiation and reflections from the environment (LN_2 shroud) could have been included in the analytical results, the differences between the analytical and experimental temperatures of the colder shield would have been larger still. The significant point to be made here is that with all the conceivable variations included, the analytical results still conservatively overpredict the shield temperatures. It is felt that this is a direct result of assuming diffuse surface properties in the analytical model. The directional emissivity of low-emissivity metallic surfaces actually help radiate more heat out the edges of the shield system and hence reduce the heat transferred through the shields. This also was demonstrated in reference 21 for two parallel rectangular surfaces. It is realized that the reflections from the highly specular (mirror-like) surfaces used could cause higher heat transfer rates for parallel surfaces, but the spacing ratios are small enough to make this increase negligible (ref. 16).

The conservatism of the diffuse analysis was not readily apparent in the previous figures because of the nature of the experimental errors and because with fewer surfaces involved, the differences would be expected to be less.

The heat transfer rates for the shield configurations given in figure 30 (also fig. 29) could not be accurately measured since the rates were extremely low. However, a rough comparison of the heat transfer rates for single- and double-sheeted shields can be made by ratioing the fourth power of the colder shield temperatures. Doing this, the analytical rates differ by about a factor of 3 and the experimental rates differ by a factor of 4 or 5. In either event, it is apparent that a considerable reduction in heat transfer rate can be obtained with minimal weight increases by adding an additional sheet of material to the shield rings.

Performance of integrated system. - With the performance of the shields known independent of the structural support system, the next step was to integrate the systems to determine the interactions between the shields and their necessary supports. Single-sheeted shields were used in order to avoid the uncertainties at the lower-temperature ranges. The first series of tests used shields pinned into their proper positions within the shield support cage with small stainless steel pins (0.01 in. (0.0254 cm) diam). See figures 8 and 9 for the arrangement of the shields and the location of the pins. The simulated payload was maintained at a controlled temperature by radiating it from the bottom

with the heater used in the previous tests.

The shield and support-cage strut temperature profiles of the pinned system are given in figure 31 along with that of the same configuration with the colder shield inverted. The normal position of the shields is as shown in figure 9. The colder shield was inverted to help determine the effect of rim temperature on the strut temperatures for the pinned systems. The analytical results for the shields do not include any interactions with the support-cage struts; and, for the normally positioned shields, the results are identical to those given previously in figure 30(a) where no support system was present. The analytical results for the struts also assumed no interactions and were determined with the analysis used for figures 24 and 25.

From figure 31(a), its apparent that pinning the shields considerably altered the temperature profiles[6] over those of freely suspended shields. For the normally-positioned colder shield, the experimental edge temperature is much higher than the shield center whereas with no strut interactions (e. g., fig. 30(a)) the edge and center temperatures were about the same. Inverting the shield caused the edge temperature of the colder shield to drop for both the analytical and experimental data. It should be noted that by inverting the shield, the temperature of the inner portions of the shield ($R/R_o < 0.5$) should have increased about 20° R (11 K) due to the slightly closer spaced sheets. The data, however, show a decrease of about 20° R (11 K). This results from the thermocouple installation technique, discussed previously, which causes high readings when the thermocoupled surface faces a warmer surface and low readings when facing a colder surface.

The effect of the widely different rim temperatures on the support-cage strut temperatures is not distinguishable from the data scatter shown on figure 31(b) but it appears small. This results because of the poor thermal bond between the struts and rims and the relatively high heat flux through the strut. Also, from the figure, it is apparent that large temperature gradients exist between the shield rims and struts for the pinned system.

These differences in temperature between the shields and the support-cage system could be advantageous or disadvantageous depending on the balance between the conductive heat transfer through the supports and the radiant heat transfer through the shield system. For systems where the conductive heat transfer is predominant, it may be beneficial to solidly connect the shields to the struts to lower the overall temperature of the structural system and hence the total heat transfer rate. This is demonstrated in figure 32 where both the shield-temperature profiles and the support-cage strut temperature profiles are

---

[6]The shield surface facing the simulated payload was contaminated with an oily substance caused by outgassing of the freshly painted payload surface. This caused higher shield temperatures than given for figure 30(a) but the conclusions made are still valid.

given for systems with good and poor thermal bonds. Shield temperature profiles are given for freely suspended shields (same as fig. 30(a)), shields that are welded within the support cage and shields that are welded and targeted. (It should be noted that the contaminated shields used in fig. 31 were replaced with new shields.) Support-cage strut temperature profiles are given for shields pinned within the cage (same as fig. 31(b)), welded shields, and welded and targeted shields. The analytical results for the shields and the struts assume no interaction between the two. In order to minimize the experimental data presented, only the arithmetic mean temperatures are presented for both the struts and the shield rims.

From the figure, it is apparent that welding the shield rings to the struts of the support cage substantially lowers the strut temperatures from those of the pinned-shield system. For example, at the location of the colder shield the local strut temperature is lowered about 40° R (22 K) below that of the pinned system. Using the experimental temperature differences at the colder end of the struts, the conductive heat transfer is calculated to be 1.9 and 1.7 Btu per hour (0.56 and 0.50 W), respectively, for the pinned shields and the welded shields. Using the experimental temperatures of the coldest shields, the radiant heat transfer rates were calculated giving a total heat transfer rate into the tank of at least[7] 2.2 Btu per hour (0.65 W) for the pinned system and about 2.4 Btu per hour (0.71 W) for the welded system. Therefore, it appears that welding the shields does not materially help the experimental model. It should be noted, however, that the high-absorptivity tank surface absorbs most of the incoming radiant heat and if the surface properties of the tank were similar to those of the shields, the radiant heat transfer would be reduced at least an order of magnitude. So for realistic surface properties, it would be beneficial to weld the shields to the struts from a thermal viewpoint. If double-sheeted shields were used for this same application, a much larger payoff would be expected for a welded system since (1) the radiant heat transfer would be still smaller and (2) the lower edge temperature of the colder double-sheeted shield would help reduce the conductive heat input further still.

Another possible means of reducing the overall heat transfer rate of an integrated system is by selectively coating (targeting) the shield rims and/or the structural members which was done for the welded system. Only the outer half of the shield rims facing the colder environment were coated with the H.T.P. The struts were completely coated due to the difficulties involved in painting the small-scale model. Had it been practically possible, only the outer half of the struts would have been painted as demonstrated pre-

---

[7]The radiant heat transfer for the pinned system was estimated from the freely suspended shield data because the pinned-shield tests were influenced by the contamination problem discussed previously. The actual pinned shield data would give a higher radiant heat flux.

26

viously for the struts shown in figure 24. The system used, however, was sufficient for demonstrating the advantages of targeting. From figure 32, it is seen that both the colder shield and the support-system temperatures are lowered by targeting the welded system. Using the experimental-shield temperatures, the radiant heat transfer is conservatively estimated to be 1. 5 Btu per hour (0. 5 W) which is about two times higher than the welded system (the heat transfer is higher because of the targeted edge). Using a simple comparison of the experimental temperature drops through the struts (281° - 166° R/320° - 166° R), it is seen that selective coating has reduced the conductive heat transfer to about 0. 75 of that for the welded system. This represents a substantial reduction in the overall heat transfer rate when realistic properties are used for the tank surface. Realistic tank properties would reduce the radiant heating at least an order of magnitude.

Although no attempt was made to analyze the interactions between the shadow shields and their necessary support structures, the data shown on figure 32 serve to illustrate both the effectiveness of a good thermal bond between the shields and struts and the effectiveness of selectively coating various portions of the system. For the system used, a good thermal bond resulted in higher radiant heating and lower conductive heating. Depending upon the balance between the two, it may or may not be desirable to provide good thermal bonds for a shield-strut system. The use of selective coatings will depend on particular configuration and the environment encountered, but, in general, they provide an economical (from weight considerations) method of improving the performance of an integrated system.

Predicted performance for full-scale system. - A rough estimate of the space performance of the shadow-shield system for the hypothetical vehicle shown in figure 26 is given in figure 33. The shield-temperature profiles and heat transfer rates are given for both single- and double-sheeted shields along with that for the tubular structural members. The analytical results assumed the shields were zero conducting and accounted for the shield rims as discussed previously. The temperature of the surrounding space environment was assumed to be at absolute zero and was nonreflecting. The shield results shown should be conservative (high) because (1) the analysis assumed diffuse surfaces which gives higher heat transfer rates and temperatures than would be expected for nondiffuse realistic surfaces and (2) the hydrogen tank ground-hold insulation was ignored (for simplicity). It should be noted that the surface temperature of the ground-hold insulation in space would be extremely low due to the low-heat transfer rates achieved by the shield systems. These low-surface temperatures could help minimize heat leaks through the various penetrations and discontinuities in the insulation.

The heat transfer rates shown are quite low but could be lowered further still with the use of a lower-emissivity material. Data from reference 4 indicates that emissivities of approximately 0. 02 can be obtained commercially for metallized films. Using a value

of 0.02 for the emissivity, the heat transfer rates would be 0.12 and 0.031 Btu per hour (0.035 and 0.0091 W), respectively, for the single- and double-sheeted shields. These rates represent the performance under optimum conditions since emissivities on the order of 0.02 may be difficult to maintain for a space-vehicle application where the shields must be handled during fabrication and are exposed to various environments prior to and during their use in space. However, if double-sheeted shields are used, it is conceivable that the low-emissivity surfaces can be maintained on the internal surfaces between common sheets since they will be isolated from the external environment. Assuming the external surfaces of the double-sheeted shields have emissivities as high as 0.1 and internal emissivities of 0.02, the radiant heat transfer rate would be approximately 0.65 Btu per hour (0.19 W), which is still extremely low. The corresponding heat transfer rate for single-sheeted shields, with an emissivity of 0.1, would be 10.8 Btu per hour (3.2 W). So it is evident that the double-sheeted shields are less sensitive to changes in external surface emissivity.

Shown on figure 33(c) are the strut temperatures and the calculated strut heat transfer rates. Also shown are the attachment points for the shields given in figures 33(a) and (b). Heat transfer rates and temperature profiles are given for (1) uncoated struts, (2) struts with zero internal emissivity, and (3) struts with an external emissivity of 1.0. For purposes of this calculation, it was conservatively assumed that the titanium strut thermal conductivity was constant at 3.5 Btu per hour per foot per ^{O}R (0.0606 W/(cm)(K)) and that the structural tubes ran directly from the payload to the hydrogen tank. Again, it is apparent that the struts can be cooled by providing good thermal bonds between the struts and shield rims. The results indicate that the strut heat transfer rates can be further decreased by selectively coating the external strut surfaces and/or decreasing the internal emissivity of the struts. The internal radiation also could be eliminated by filling the structural tubes with a low-density foam or by using internal shields. More importantly, the assumption of titanium struts and good thermal bonds at both the payload and the LH_2 tank is quite conservative. With the use of thermal blocks and fiberglass support members, the strut heat leaks can be reduced by at least an order of magnitude.

A rough idea of the weight penalties involved with the use of the shadow shield system can be obtained by using the heating rates given on figure 33. Assuming single-sheeted shields (0.42 Btu/hr or 0.12 W) and foam-filled struts (3.3 Btu/hr or 0.97 W), the total hydrogen boiled off in 200 days is about 90 pounds (41 kg). The weight of the shadow shield system is estimated to be about 94 pounds (42.6 kg) including 50 pounds (22.7 kg) for ground-hold insulation and 16 pounds (7.2 kg) for lengthening the stage 1 foot (30.5 cm) giving a total weight penalty of 184 pounds (83.5 kg). This does not include the boil-off through the aft end of the tank, which is practically negligible, or the weight penalties involved with the liquid oxygen tanks.

Since multilayer insulations represent the most efficient insulations currently available, it is of interest to examine the insulation required to provide the same protection as that afforded by the shadow shields for the vehicle selected. This is demonstrated in figure 34 for two values of thermal conductivity with the lower value being representative of about the best insulation currently available (ref. 22). The upper value is included to demonstrate the effect of higher conductivity because most applications of the multilayer insulation to date have resulted in much higher thermal conductivities (e.g., ref. 5 quotes 5.5×10^{-5} to 15×10^{-5} Btu/(hr)(ft)(^{O}R) or 9.5×10^{-7} to 26×10^{-7} W/(cm)(K)). It is apparent that large thicknesses of insulation are required to match the performance of the shadow shields. Also demonstrated on figure 34 is the effect of using a single shield to help reduce the insulation requirements on a multilayer-insulated tank. For this particular case the insulation thicknesses can be reduced by a factor of 2 or more depending on the heat transfer rate desired.

An estimate of the weight penalty of an all-multilayer-insulated tank can be made by assuming a one-to-one trade-off between boil-off weight and insulation weight. Using the curve for the lower value of thermal conductivity and a density of 2.5 lb/ft^3 (40 kg/m^3) results in an insulation weight (and boil-off weight) of 37 lb (16.8 kg) or 1.4 inches (3.6 cm) of insulation. These results are for the same spacing as that of the shadow shield system since the increased stage length also benefited the multilayer system. Assuming the same heat leak through the struts and the same weight penalties for the ground-hold insulation, the total weight penalty for the multilayer-insulated system is 220 lb (100 kg). Although neither the multilayer or shadow shield system has been truly optimized, the magnitude of the weight penalties indicates that the shadow shields can be useful for this particular mission. For longer duration missions or missions where the heat leak must be kept to a minimum, the shadow shields will be still more beneficial especially if the support heat leaks can be reduced (e.g., using fiberglass supports).

It should be noted, however, that the results given for both figures 33 and 34 are for a sun-oriented vehicle. Most missions will require that the vehicle be misoriented occasionally for various reasons, for example, midcourse correction maneuvers. During these periods the ground-hold insulation will have to include enough multilayer insulation or other high performance insultion to maintain low heating rates. If long periods of time are spent nonalined with the sun or in near-planetary orbits, the advantages of the shadow shields will be mitigated since they depend upon a unidirectional heat source. For these situations the use of multilayer insulation will result in lower weight penalties. There are also many situations between complete solar orientation and no orientation where the shadow shields can be used to help reduce the insulation requirements of a multilayer-insulated system or to help augment some other primary thermal protection system.

CONCLUDING REMARKS

Summarizing, the effects of various basic parameters on shadow-shield performance were examined including number of shields, spacing, emissivity, lateral conductance, and targeting. The results were as follows:

1. Experiments performed on the relatively thick, high-lateral conductance copper shields demonstrated that the radiant heat transfer between two bodies can be reduced by increasing the number of shields, increasing the spacing between shields and/or decreasing the emissivity of the shields. The effects of shield number were seen to be more pronounced as the emissivity was lowered. Also for multiple shield systems, lowering the emissivities resulted in a stronger effect of shield spacing. The analysis given in reference 8 which assumed uniform radiosity surfaces (simplified-diffuse) was found to be adequate for the higher emissivity shields, but considerably underestimated the heat transfer for lower-emissivity shield systems where the reflected term in the radiosity becomes significant. The more complex exact-diffuse analysis (ref. 16), which assumed diffuse emissions and reflections for nonuniform radiosity surfaces, adequately predicted the shield performance for all the basic tests including those with the glass-blasted copper surfaces.

2. Experiments on shields with varying lateral conductance (kt/R_o^2) demonstrated that the exact-diffuse analysis can accurately predict the shield performance and that relatively large-temperature gradients, from shield center to edge, can be encountered with low-conductance shields. The local-shield temeratures for the low-conductance shields were typically highest in the center of the shield and decrease monotonically outward toward the shield edge. It was determined both analytically and experimentally that decreasing the shield-lateral conductance caused an increase in heat transfer rate. It was also shown that the relative difference between the heat transfer rates for high-conductance and low-conductance shields increases with decreasing emissivity. For the three-shield system tested, shields with emissivities on the order of 0.94 gave a 20 percent difference between near-zero and near-infinite conductance shields, while shields with an emissivity of 0.03 are calculated to give a 50-percent difference. Although not experimentally verified, the thermal performance of a shield system, with equivalent boundary temperatures and surface properties, should be identical for any size (diameter) system as long as the relative shield spacings (L/R_o) and lateral conductance (kt/R_o^2) remain constant.

3. The targeted shield tests demonstrated that selective coating of annular areas of a shield can provide an effective method of controlling the shield-temperature profile. This concept could be used to tailor shield temperatures to make them compatible with some other system requirement.

The effort applied toward practical shields pointed out the following:

1. The use of a peripheral ring with a shield material stretched over and secured to it (single-sheeted shield) provided a practical lightweight method of constructing a shadow shield. The exact-diffuse analysis of reference 16 for flat-disk shields conservatively predicted the performance of the practical shields, despite the discontinuity imposed by the support ring. The shield-temperature profiles were found to be very sensitive to the relative location of the high-emissivity support rings (targeted edges).

2. The application of shield material to both sides of a peripheral ring, forming a double-sheeted shield, provides a shield that far outperforms the single-sheeted shield for little increase in shield weight. Experiments on a double-sheeted shield demonstrated that increasing the emissivity of the external surface by a factor of about 30 (while retaining the same internal emissivities) only caused a factor of 2.5 increase in heat transfer rate. This suggests that the double-sheeted shields may be especially beneficial in situations where the external surface properties may be deteriorated by environmental effects (possible meteoroid errosion). The analytical results for the two double-sheeted shields predicted higher temperatures than measured and it is felt that the directional properties of the shield material caused the lower experimental temperatures. The temperatures of the shield rims, where both the colder and warmer sheets were commonly attached, could not be accurately predicted since the analysis assumed no contact between sheets. From an engineering standpoint, however, the diffuse analysis should be adequate for conservatively predicting the performance of compact shield systems.

The effort applied toward shield supports and the integration of supports and shields for the scale-model system pointed out the following:

1. The heat transferred through tubular structural members connecting warmer components with a cryogenic tank can be reduced significantly by selectively coating the tube surfaces with a high-emissivity coating.

2. The integration of a shield system and a support system does not necessarily cause a deterioration in overall system performance. Providing a good thermal contact between shield rims and their necessary supports can actually enhance the overall system performance in some situations. The best type of thermal bond to be used between the shields and their supports depends upon the relative magnitude of the radiant heat transfer from the shields and the conductive heat transfer through the supports. Although no analysis was made of the interaction between the shields and supports, the use of the separate analyses for the shields and for the supports can assist in determining how and where to attach the shields.

3. Selectively coating the scale-model system significantly lowered the temperatures of the shield struts and pointed out a means of lowering the overall heat transfer rate. Although the particular coating pattern used was not optimized, it demonstrated the utility of selective coating and a lightweight method of temperature control.

The estimates made for the shield system of a hypothetical vehicle on a 200-day Mars mission indicated that shadow shields provide an efficient method of thermally protecting the on-board cryogenic tanks. Their use depends upon solar orientation and, generally, would be most useful for long-duration sun-oriented missions. On missions where long times are spent nonoriented or in near-planetary orbits they may still be useful for augmenting other primary thermal-protection systems.

The analysis used throughout the report (ref. 16) assumed diffusely emitting and reflecting surfaces despite the fact that typical shield materials (1) will have properties that are directionally dependent and (2) will reflect somewhat specularly. However, both of these real-surface-characteristic properties could result in a lower heat transfer rate when taken into account in a system design. Most metallic surfaces emit and reflect more strongly at high angles to the surface normal which should result in lower heat transfer than those given by the report analysis. Specular reflections can cause higher heat transfer rates than diffuse reflections for widely-spaced, flat-parallel disks, but they also can cause lower rates where curved surfaces are involved such as between a flat shield and an ellipsoidal tank.

Lewis Research Center,
National Aeronautics and Space Administration,
Cleveland, Ohio, May 20, 1968,
124-09-05-12-22.

APPENDIX A

SYMBOLS

A   surface area, ft^2 (m^2)

B   Gebhart's absorption factor (fraction of total energy emitted by one surface that is absorbed by another)

D   diameter, in. (cm)

F   view factor

k   thermal conductivity, Btu/(hr)(ft)(^{O}R) (W/(cm)(K))

L   distance between heat sources and heat sink or total length of strut, in. (cm)

N   number of shields

n   number of annular elements on shield

$\dot{Q}$ heat transfer rate, Btu/hr (W)

R   radial distance from shield center, in. (cm)

s   intermediate distances (e.g., between shields), in. (cm)

T   absolute temperature, ^{O}R (K)

t   shield thickness, in. (cm)

X   distance from cold end of strut, in. (cm)

α absorptivity

ϵ emissivity

ρ reflectivity

σ Stefan-Boltzman constant, 0.1713×10^{-8} Btu/(hr)(ft^2)(^{O}R^4) (5.6699×10^{-12} W/(cm^2)(K^4))

Subscripts:

an   analytical

c-in   conducted in

c-out   conducted out

en   environmental

ex   experimental

ext   external

H	heater
in	internal
j	refers to an element upon which a heat balance is being made
k	refers to other elements in an enclosure for a system of shields
l	refers to other elements in an enclosure for a tube
o	external surface of strut or when used in conjunction with a shield, it represents the shield radius
r-en	radiated from surrounding environment
r-in	radiated from internal surface
s	strut
T	tank
x	refers to a position along the length of a strut

APPENDIX B

ANALYSIS

The analytical results for the shadow shields used throughout this report utilized the analytical (exact-diffuse) model presented in reference 16 for flat-disk shadow shields. Basically, this model assumed that (1) the shields were made up of n concentric isothermal rings, (2) radiosity was constant across any given ring but varied from ring to ring across the shield, (3) surfaces were diffusely emitting and reflecting, (4) shield absorptivities and emissivities were separate independent functions of temperature and/or position with the reflectivity defined as $1 - \alpha$, (5) no temperature gradient existed through the thickness of the shield and no radiation to or from the shield edge, and (6) the shield thermal conductivity could be temperature dependent.

A sketch of the analytical model is given in figures 35 and 36. Figure 35 defines the radiant heat transfer to the jth (annular) element of a shield surrounded by adjacent surfaces (or shields), while figure 36 includes both radiation and conduction for the jth element. The terms $B_{1j}, B_{2j} \ldots B_{nj}$ are defined as:

$$B_{1j} = \alpha_j F_{1j} + \rho_1 F_{11} B_{1j} + \rho_2 F_{12} B_{2j} + \cdots + \rho_n F_{1n} B_{nj}$$

$$B_{2j} = \alpha_j F_{2j} + \rho_1 F_{21} B_{1j} + \rho_2 F_{22} B_{2j} + \cdots + \rho_n F_{2n} B_{nj}$$

$$.$$
$$.$$
$$.$$

$$B_{nj} = \alpha_j F_{nj} + \rho_1 F_{n1} B_{ij} + \rho_2 F_{n2} B_{2j} + \cdots + \rho_n f_{nn} B_{nj}$$

The term B_{ij} represents the fraction of total energy emitted by i that is absorbed by the jth surface. This also includes the energy from i that eventually reaches j by multiple reflections within the enclosure. These terms are the absorption factors used in Gebhart's method for calculating the radiant heat exchange in an enclosure (e.g., see ref. 19, pp. 121-123). The use of an absorptivity independent of the emissivity in the analysis (of ref. 16) does not make the calculation for nongray surfaces practically possible since absorptivity also depends upon the wavelength of the incoming radiation which in turn is a function of all the elemental surface temperatures in the enclosure. The utility of the analysis, however, lies in the added flexibility provided for simulating real-

istic shield systems with the flat-disk analytical model used. For the most part, the results in this report do, in fact, assume gray surfaces, which is a reasonable assumption for the small-temperature differences experienced between adjacent surfaces.

Under steady-state conditions, the net radiant heat input will equal the net heat conducted from the element; so if the temperatures and properties of the surrounding surface elements are known, the temperature of the jth surface can be determined. Similar energy balances can be made on each annular ring in the shield array and thereby determine the temperature and heat transfer relations for the entire system. The solution of the system of equations is quite involved and is not presented here. The complete analysis of this problem and a computer program for its solution are given in reference 16.

It should be noted that if each shield contains only one surface element, the subsequent solution of the system of equations agrees with the results of the uniform radiosity solution presented in reference 8. Reference 16 demonstrates that the uniform radiosity assumption can seriously underestimate the heat transfer rate for low emissivity shields at certain low spacings. This is also demonstrated for some of the experimental results of this report.

Also included in the current report are analytical results for heat transferred through tubular support members. Again the complete analysis for the support members is presented in reference 16 and is only briefly reviewed here for clarity. A sketch of the model used and the heat balance for a segment of tube is given in figure 37.

Gebhart's method was used to determine the internal radiation in the strut. The basic assumptions for this model were: (1) the environmental surroundings had a uniform temperature with an emissivity of one and a reflectivity of zero, (2) all surfaces were gray and were diffusely emitting and reflecting, (3) there are no radial or circumferential temperature gradients in the strut, and (4) the strut material was homogeneous and had a temperature dependent thermal conductivity.

REFERENCES

1. Hnilicka, M. P.: Engineering Aspects of Heat Transfer in Multilayer Reflective Insulation and Performance of NRC Insulation. Advances in Cryogenic Engineering. Vol. 5, K. D. Timmerhaus, ed., Plenum Press, Inc., 1960, pp. 199-208.

2. Matsch, L. C.: Advances in Multilayer Insulations. Advances in Cryogenic Engineering. Vol. 7, K. D. Timmerhaus, ed., Plenum Press, Inc., 1962, pp. 413-418.

3. Knoll, Richard H.; and Oglebay, Jon C.: Lightweight Thermal Protection Systems for Space Vehicle Propellant Tanks. Paper No. 746C, SAE, Sept. 1963.

4. Anon.: Advanced Studies on Multi-layer Insulation Systems. Rep. ADL-67180-00-04, Arthur D. Little, Inc. (NASA CR-54929), June 1, 1966.

5. Sterbentz, W. H.; and Baxter, J. W.: Thermal Protection System For a Cryogenic Spacecraft Propulsion Module, Vol. 2. Rep. LMSC-A794993, Vol. 2, Lockheed Missiles and Space Co. (NASA CR-54879, Vol. 2), Nov. 15, 1966.

6. Hall, Charles F.; Nothwang, George J.; and Hornby, Harold: Solar Probes - A Feasibility Study. Aerospace Eng., vol. 21, no. 5, May 1962, pp. 22-30.

7. Lundholm, J. G., Jr.; Prohaska, E. S.; Hoyer, S.; and Averell, J.: A Close Approach Solar Probe Design Feasibility and Mission Study. Paper No. 64-496, AIAA, June 1964.

8. Smolak, George R.; Knoll, Richard H.; and Wallner, Lewis E.: Analysis of Thermal-Protection Systems for Space-Vehicle Cryogenic-Propellant Tanks. NASA TR R-130, 1962.

9. Jones, L. R.; and Barry, D. G.: Lightweight Inflatable Shadow Shields for Cryogenic Space Vehicles. J. Spacecraft and Rockets, vol. 3, no. 5, May 1966, pp. 722-728.

10. Nichols, Lester D.: Effect of Shield Position and Absorptivity on Temperature Distribution of a Body Shielded from Solar Radiation in Space. NASA TN D-578, 1961.

11. Nothwang, George J.; Arvesen, John C.; and Hamaker, Frank M.: Analysis of Solar-Radiation Shields for Temperature Control of Space Vehicles Subjected to Large Changes in Solar Energy. NASA TN D-1209, 1962.

12. Arvesen, John C.; and Hamaker, Frank M.: Effectiveness of Radiation Shields for Thermal Control of Vehicles on the Sunlit Side of the Moon. NASA TN D-2130, 1964.

13. Arvensen, John C.: Effectiveness of Solar Radiation Shields For Thermal Control of Space Vehicles Subject to Large Changes in Solar Energy. Symposium on Thermal Radiation of Solids. S. Katzoff, ed. NASA SP-55 (AFML-TDR-64-159), 1965, pp. 549-557.

14. Barry, D. G.; and Goodman, E. H.: Thermal Protection Systems for Cryogenic Propellants on Interplanetary Space Vehicles. Vol. IV: Analytical and Experimental Study of Certain Thermal Analysis Techniques. Rep. FZA-416-IV, General Dynamics/Fort Worth (NASA CR-79991), Sept. 21, 1966.

15. Knoll, Richard H.; Bartoo, Edward R.; and Boyle, Robert J.: Shadow Shield Experimental Studies. Presented at the Conference on Long-Term Cryo-Propellant Storage in Space, NASA Marshall Space Flight Center, Huntsville, Ala., Oct. 12-13, 1966.

16. Boyle, Robert J.; and Knoll, Richard H.: Thermal Analysis of Shadow Shields and Structural Members in a Vacuum. NASA TN D-4876, 1968.

17. Anon.: Liquid Propellant Losses During Space Flight. Rep. 65008-00-04, Arthur D. Little, Inc. (NASA CR-53336), Oct. 1964.

18. Curtis, Henry B.; and Nyland, Ted W.: Apparatus for Measuring Emittance and Absorptance and Results for Selected Material. NASA TN D-2583, 1965.

19. Wiebelt, J. A.: Engineering Radiation Heat Transfer. Holt, Rinehard & Winston, Inc., 1966.

20. Caren, R. P.: Low-Temperature Emittance Determinations. Paper No. 65-703, AIAA, Sept. 1965.

21. Viskanta, Raymond; Schornhorst, James R.; and Toor, Jaswant S.: Analysis and Experiment of Radiant Heat Exchange Between Simply Arranged Surfaces. Purdue Univ. (AFFDL-TR-67-94, DDC No. AD-655335), June 1967.

22. Glaser, Peter E.; Black, Igor A.; Lindstrom, Richard S.; Ruccia, Frank E.; and Wechsler, Alfred E.: Thermal Insulation Systems. NASA SP-5027, 1967.

TABLE I. - DETAILS OF SHADOW SHIELDS USED IN EXPERIMENTAL PROGRAM

Shield designation	Shield material	Thickness		Surface finish	Emissivity at room temperature or as a function of temperature (T), ^{O}R (K)	Assumed thermal conductivity		Lateral conductance at room temperature, $kt/(R_o^2)$		Remarks
		in.	cm			Btu/(hr)(ft)(^{O}R)	W/(cm)(K)	Btu/(hr)(ft^2)(^{O}R)	W/(cm^2)(K)	
I	Copper	0.0625	0.1588	High-temperature paint (H. T. P.)[a]	~0.94 (see fig. 12)	230	3.98	4.25	2.4×10^{-3}	Shield diameter was 12.75 inches (32.4 cm). (All shields listed have same diameter.)
II	Copper	0.0625	0.1588	Glass-blasted	$0.23625 + 4.25 \times 10^{-5}$ T $(0.23625 + 7.66 \times 10^{-5}$ T)	230	3.98	4.25	2.4×10^{-3}	A slurry of air and fine glass beads was used to provide a clean diffuse-appearing surface.
III	Aluminum	0.040	0.1015	High-temperature paint (H. T. P.)	~0.94 (see fig. 12)	80	1.385	0.95	5.4×10^{-4}	--------------------
IV	Stainless steel (304)	0.090	0.02285	High-temperature paint (H. T. P.)	~0.94 (see fig. 12)	8.5	0.147	2.26×10^{-1}	1.28×10^{-4}	--------------------
V	Stainless steel (304)	0.015	0.0381	High-temperature paint (H. T. P.)	~0.94 (see fig. 12)	8.5	0.147	3.77×10^{-2}	2.13×10^{-5}	Shield rigidized by stamping perpendicular ridges across shield.
VI	Mylar	0.002	0.0051	High-temperature paint (H. T. P.)	~0.94 (see fig. 12)	0.072	0.00124	4.25×10^{-5}	2.4×10^{-8}	Mylar was cemented to a stainless-steel circumferential support ring. Diameter, 12.75 inches (32.4 cm); wall, 0.1 by 0.2 inch (0.254 by 0.508 cm).

VII	AMA	0.0017	0.0043	Clean, highly-reflective	$-0.0023 + 5.06 \times 10^{-5} T$ $(0.0023 + 9.1 \times 10^{-5} T)$	80 and 0.072	1.385 and 0.00124	1.66×10^{-2}	9.38×10^{-6}	Aluminum-Mylar-aluminum laminate cemented to ring (same as VI). Aluminum, 0.00035 inch (0.00089 cm); Mylar, 0.001 inch (0.00254 cm).
VIII	AMA targeted	0.0017	0.0043	Same as VII with black band on one side and the other side completely black (H.T.P.)	Same as VII with black surface emissivities given by figure 12.	80 and 0.072	1.385 and 0.00124	1.66×10^{-2}	9.38×10^{-6}	Same as VII with a 1-inch (2.54-cm) band of high-temperature paint applied to one edge. Opposite side of shield was completely covered with H.T.P.
IX	Aluminized Mylar	0.00025	0.000635	Clean, highly-reflective	~0.03 (see fig. 13)	130 and 0.072	2.25 and 0.00124	1.41×10^{-4}	8.0×10^{-8}	Double-aluminized Mylar (900 Å of aluminum) cemented to a stainless steel 12.75-inch (32.4-cm) diameter "O" ring. Ring was 0.125 inch (0.317 cm) in diameter and 0.01 inch (0.0254 cm) thick.
X	Aluminized Mylar, double-sheeted shield	0.00025	0.000636	Clean, highly-reflective	~0.03 (see fig. 13)	130 and 0.072	2.25 and 0.00124	1.41×10^{-4}	8.0×10^{-8}	Double-aluminized Mylar cemented to both sides of "O" ring, completely enclosing support ring.
XI	Aluminized Mylar, double-sheeted shield	0.00025	0.000635	Same as X with external surface coated with H.T.P.	~0.030 (see fig. 13) Int. ~0.94 (see fig. 12) Ext.	130 and 0.072	2.25 and 0.00124	1.41×10^{-4}	8.0×10^{-8}	Same as X except external surfaces of shield were coated with the high-temperature paint.
XII	Aluminized Mylar, double-sheeted shield	0.00025	0.000635	All surfaces coated with H.T.P.	~0.94 (see fig. 12)	130 and 0.072	2.25 and 0.00124	1.41×10^{-4}	8.0×10^{-8}	Same as X except all surfaces were coated with the high-temperature paint.

[a]Paint with an emissivity near unity and capable of maintaining predictable properties up to 810° R (450 K).

TABLE II. - ACCUMULATED RANDOM ERRORS FOR SEVERAL SHIELD CONFIGURATIONS

[Probable error in high-temperature-paint emissivity, ± 5 percent for $T \leq 520^{\circ}$ R (289 K), ± 3 percent for $T = 800^{\circ}$ R (445 K); probable error in LN_2 tank emissivity, ± 5 percent; and probable error in measuring boiloff, ± 1 percent.]

Number of shields	Surface finish	Total spacing, L/R_o	Probable error in measured heat transfer rate, percent	Probable error in temperature of coldest shield, percent
Zero	----------------------------	0.01 to 1.0	± 6.2	----
1	High-temperature paint (fig. 12)	0.157 to 1.256	± 7.5	± 0.9
1	Glass-blasted copper	0.157 to 1.256	± 9	$\pm .9$
3	High-temperature paint (fig. 12)	0.157	± 9	± 1.1
3	High-temperature paint (fig. 12)	1.256	± 12	± 1.7
3	Glass-blasted copper	0.157	± 11.3	± 1.2
3	Glass-blasted copper	0.628	± 16.8	± 2.1
5	High-temperature paint (fig. 12)	0.941	± 13.4	± 2.3
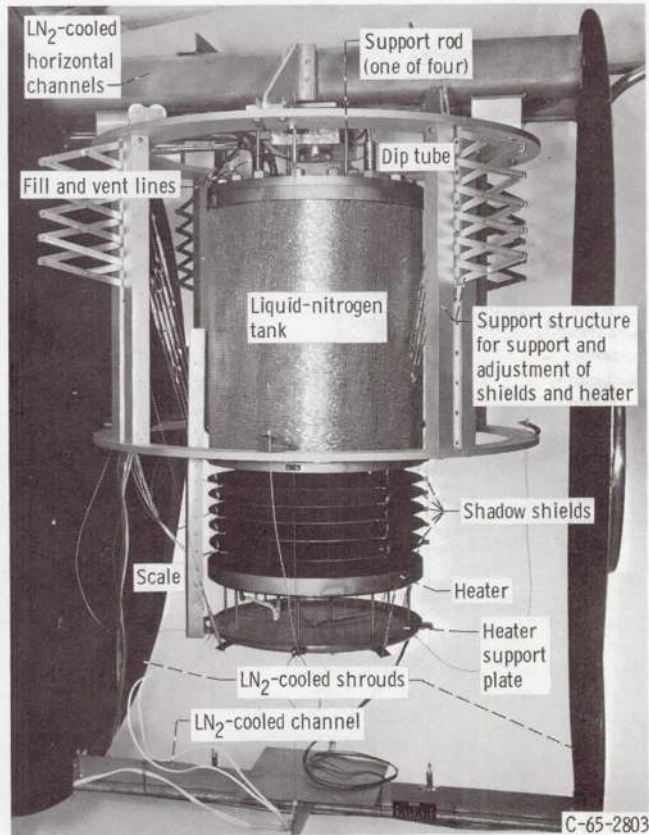
Figure 1. - Apparatus used for a five-shield test.
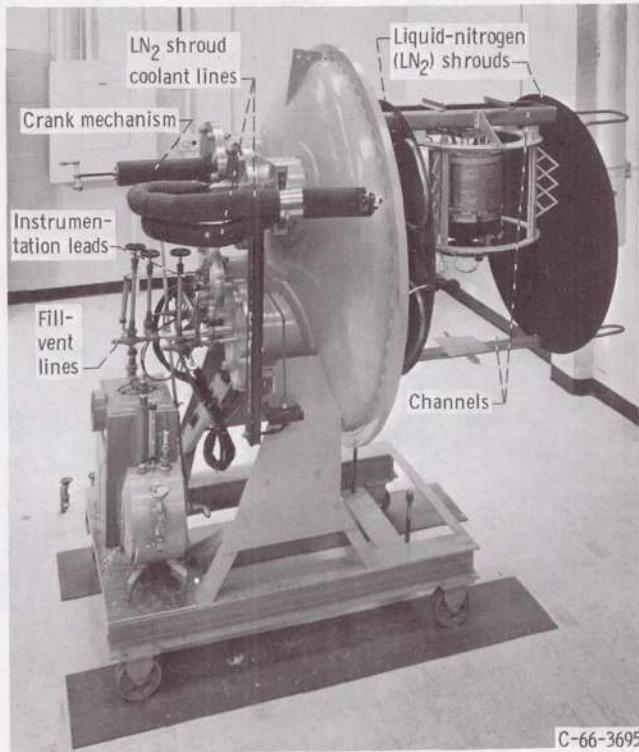
Figure 2. - Overall view of experimental apparatus connected to vacuum chamber door.
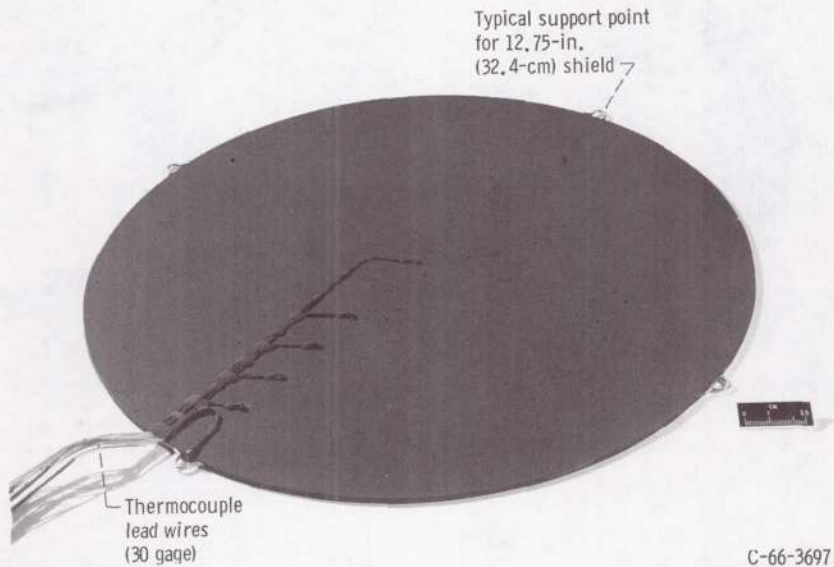
Figure 3. - Typical construction and instrumentation used for relatively thick copper, stainless-steel, and aluminum shadow shields (shields I, II, III, and IV).
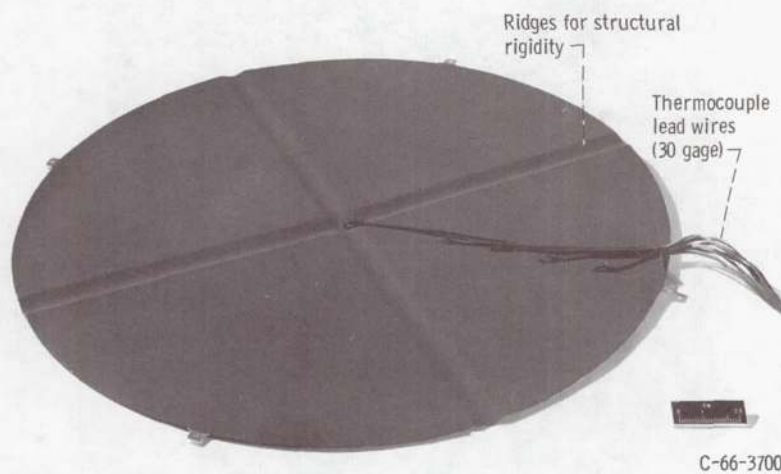
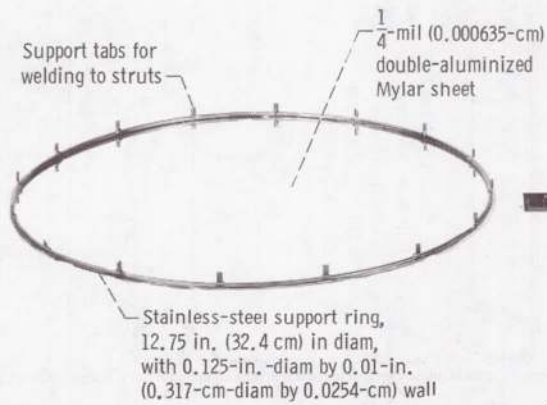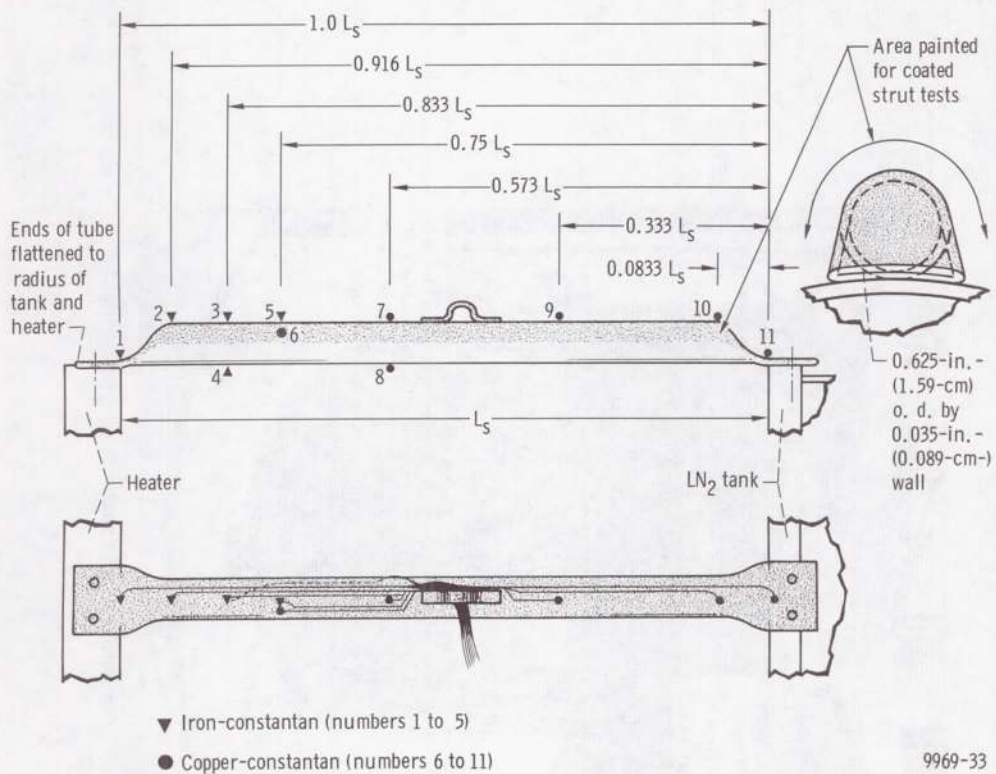Figure 4. – Construction method for 0.015-inch (0.0381-cm) stainless-steel shield (shield V).
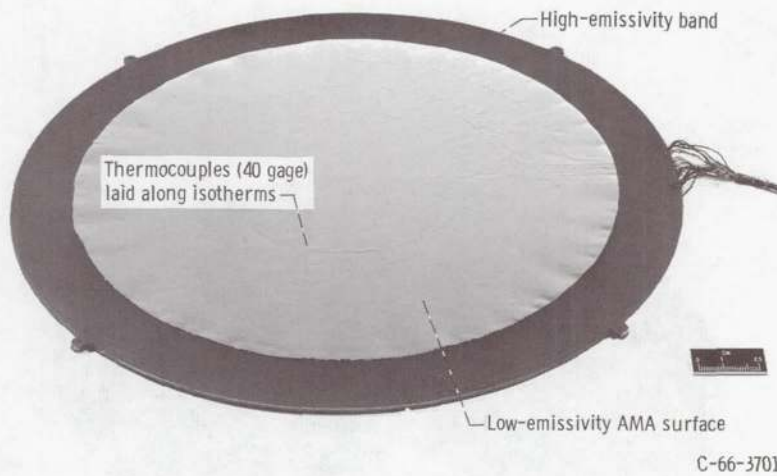
Figure 5. – Laminated aluminum-Mylar-aluminum (AMA) shield with targeted band (shield VIII). Underside of shield contains thermocouples and is coated with high-emissivity paint.

Support tabs for welding to struts

$\frac{1}{4}$-mil (0.000635-cm) double-aluminized Mylar sheet

Stainless-steel support ring, 12.75 in. (32.4 cm) in diam, with 0.125-in.-diam by 0.01-in. (0.317-cm-diam by 0.0254-cm) wall

C-67-4050

Figure 6. – Single-sheeted shield with support tabs (representative of shield IX).

1.0 L_s

0.916 L_s

0.833 L_s

0.75 L_s

0.573 L_s

0.333 L_s

0.0833 L_s

Area painted for coated strut tests

Ends of tube flattened to radius of tank and heater

L_s

Heater

LN$_2$ tank

0.625-in.- (1.59-cm) o. d. by 0.035-in.- (0.089-cm-) wall

▼ Iron-constantan (numbers 1 to 5)

● Copper-constantan (numbers 6 to 11)

9969-33

Figure 7. – Schematic diagram of support tubes and location of 30-gage thermocouples.

45

√2 ellipsoidal tank with multilayer insulation on sides

Copper pads

Support struts

Shadow shields

Simulated payload

Hose clamp for securing shield system to tank

C-66-3696
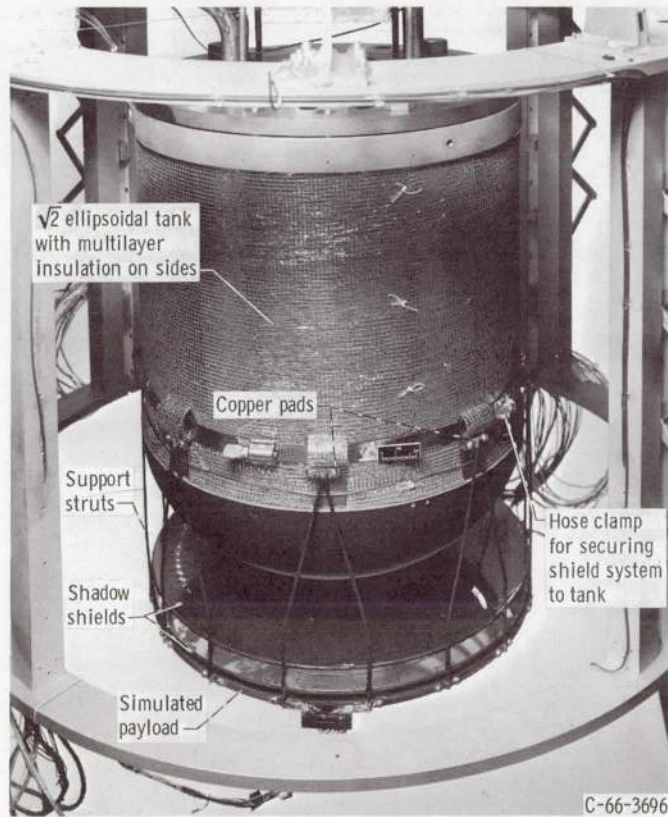
Figure 8. - Scale model of practical shadow shield system, welded and targeted.

Typical pin location for pinned shield tests

0.10-in. (0.254-cm) o. d. stainless-steel tubular strut; wall thickness, 0.012-in. (0.0305 cm)

0.16 in. (0.407 cm) to bottom of tank

0.00025-in. (0.000635-cm) double-aluminized Mylar

12.75-in. (32.4-cm) stainless-steel ring, 0.125-in.-diam by 0.010-in. (0.137-cm-diam by 0.0254-cm) wall

Weld points for support tabs

1.0 (2.54)

0.74 (1.88)

0.48 (1.22)

0.223 (0.56)

0.25-in. (0.635-cm) copper plate (simulated payload)

Figure 9. - Shield construction and method of mounting for integrated shadow shield system. (Dimensions are in inches (cm).)

0.00025-in.
(0.000635-cm-)
aluminized
Mylar sheet

Ends of 40 gage thermocouples
covered with aluminized
Mylar patches

Support tabs for
welding to struts

C-66-3699
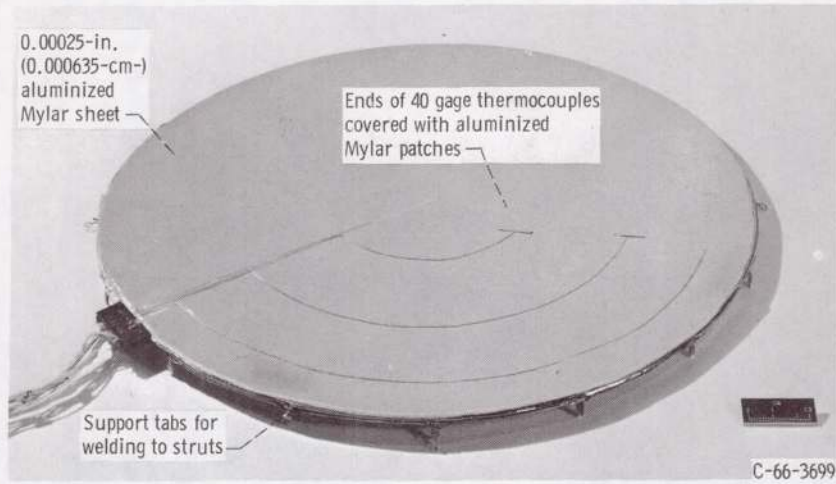
Figure 10. - Double-sheeted shield with structural support welding tabs.

D   A, C   B

Simulated
payload

A

D   B

C
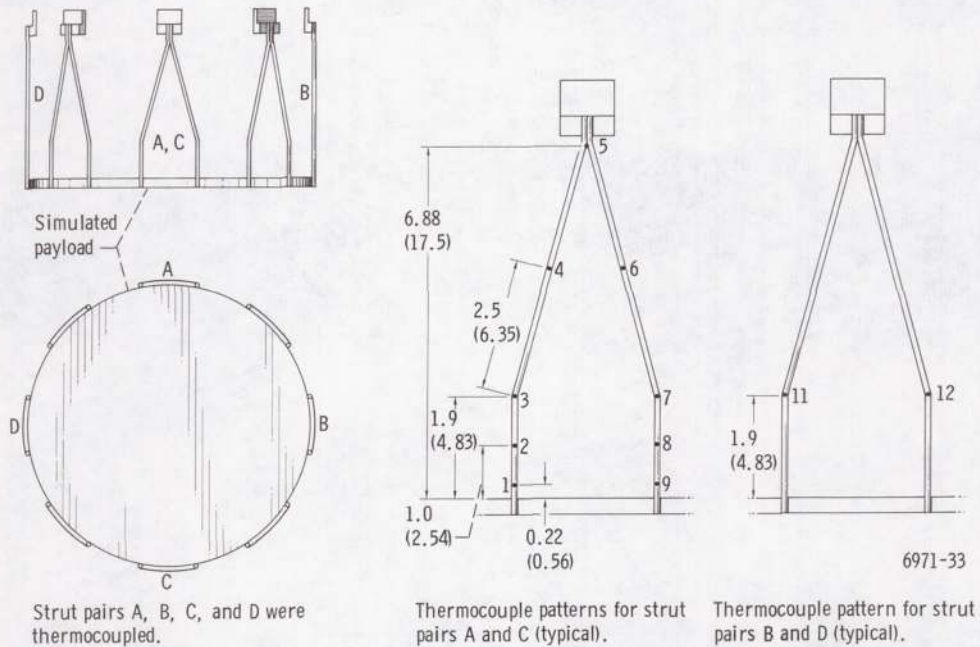
Strut pairs A, B, C, and D were
thermocoupled.

6.88
(17.5)

2.5
(6.35)

1.9
(4.83)

1.0
(2.54)

0.22
(0.56)

5

4   6

3

2

1

7

8

9

Thermocouple patterns for strut
pairs A and C (typical).

1.9
(4.83)

11   12

6971-33

Thermocouple pattern for strut
pairs B and D (typical).

Figure 11. - Location of 40-gage thermocouples for structural support cage of scale model. Thermocouples 1, 2, 8,
and 9 were iron-constantan. Thermocouples 3 to 7, 11, and 12 were copper-constantan. (Dimensions are in
inches (cm).)
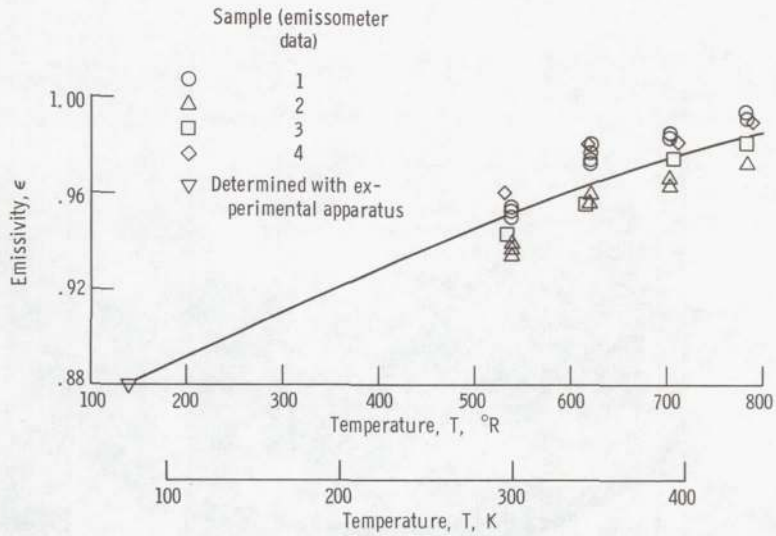
Figure 12. - Emissivity as function of temperature for high-temperature paint. Standard deviation, ±0.0089.
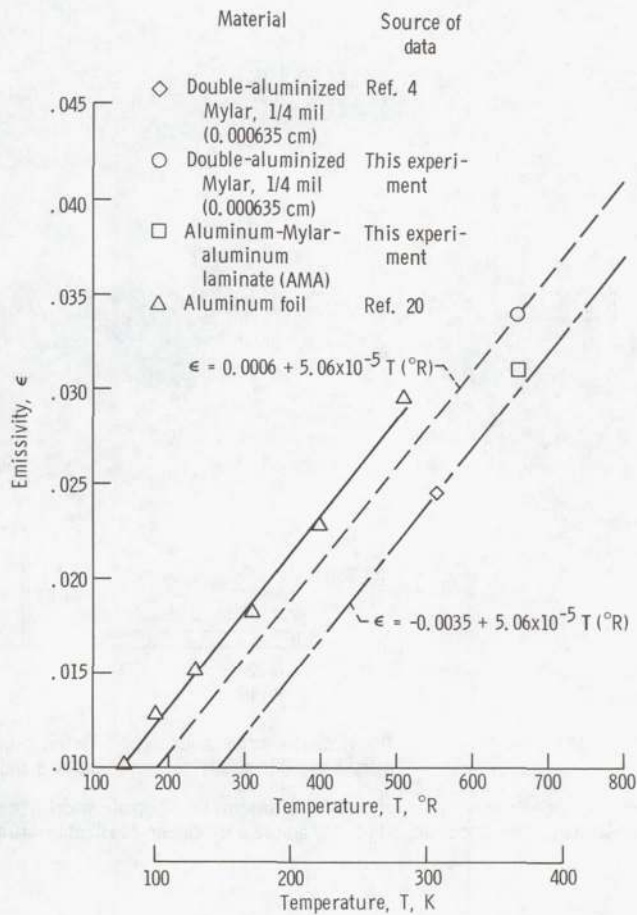
Figure 13. - Emissivity of double-aluminized Mylar and aluminum foil.
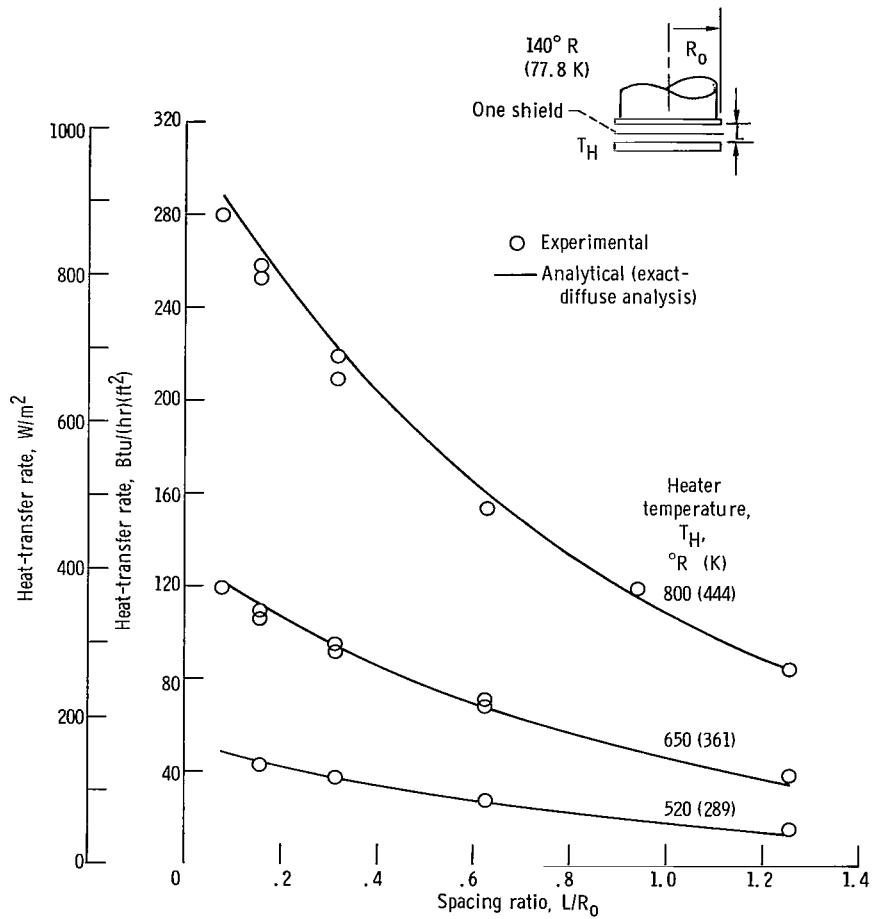
Figure 14. - Heat-transfer rate as function of spacing ratio and heat-source temperature for one shadow shield (shield I).

49
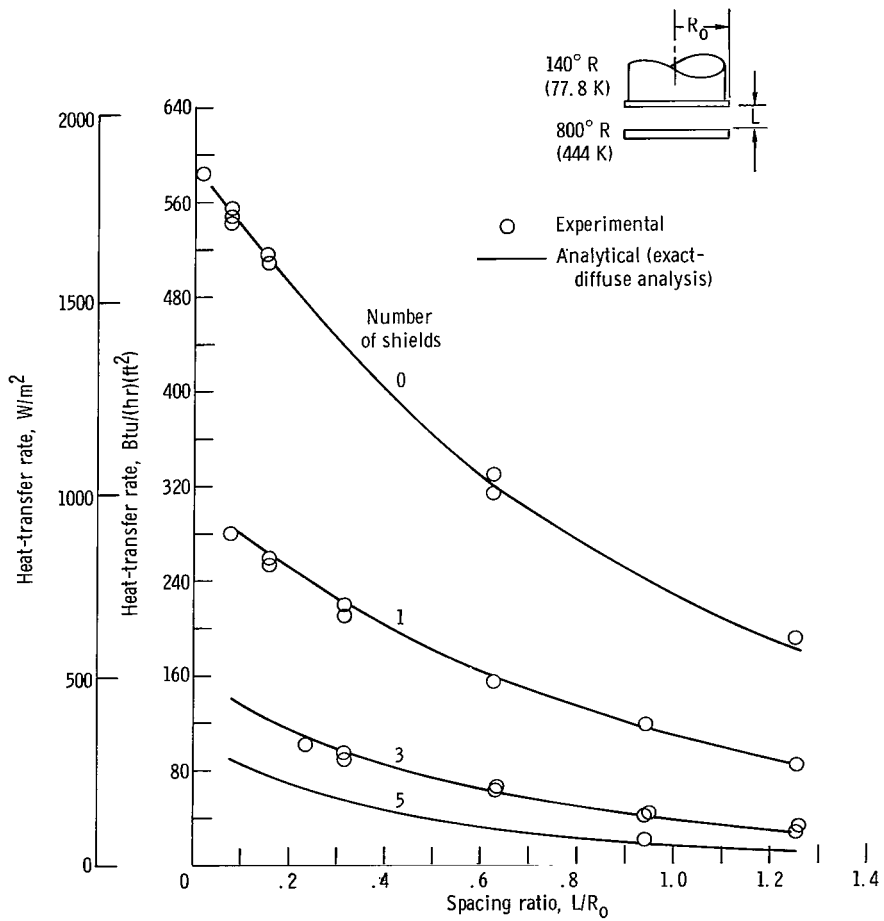
Figure 15. - Effect of shield number and spacing ratio on shadow shield heat-transfer rate. (Shield I.)
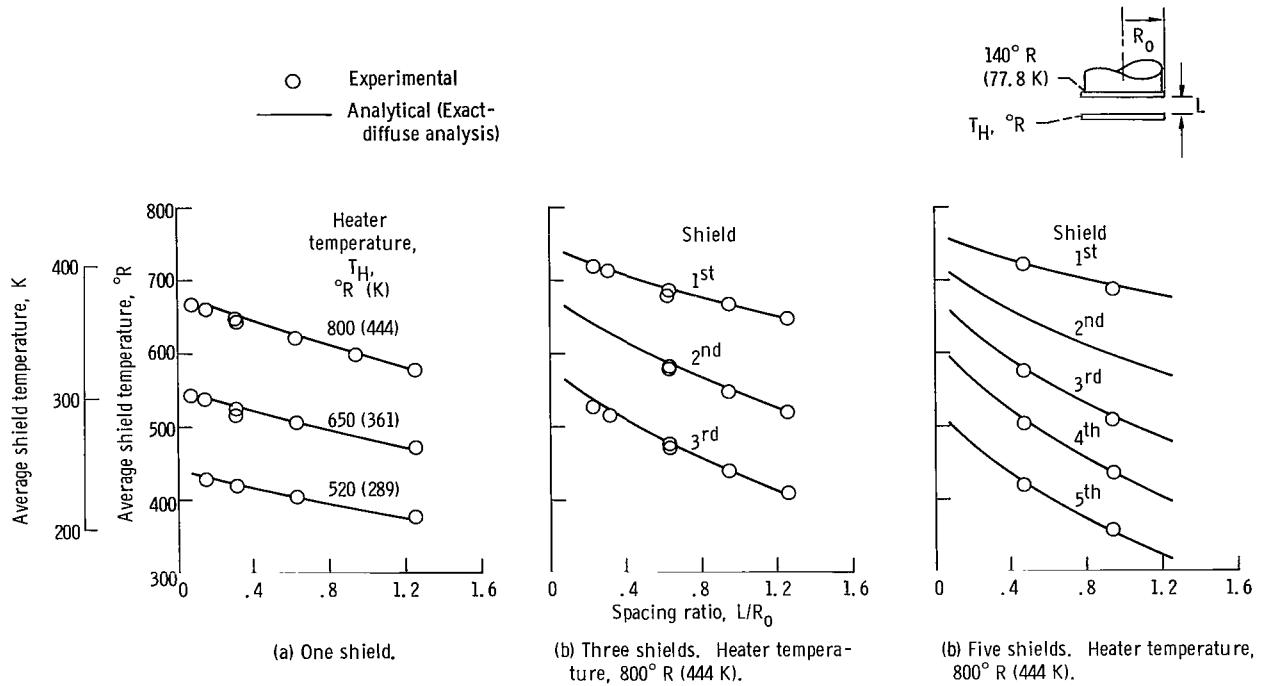
Figure 16. – Average shield temperatures for high-conducting, high-emissivity shield configurations (shield I).
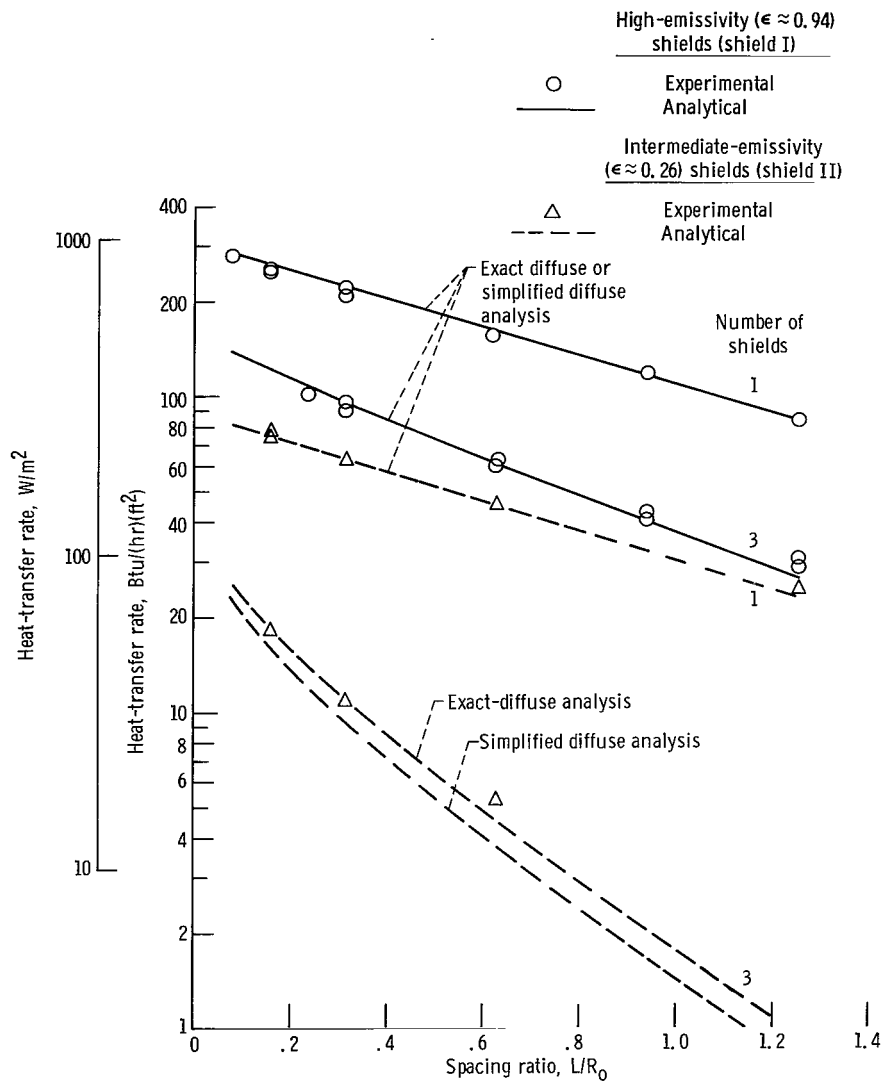
Figure 17. – Effect of shield emissivity and spacing ratio on heat-transfer rate for high-conducting shields (shields I and II). (Heater temperature, 800° R (444 K)).
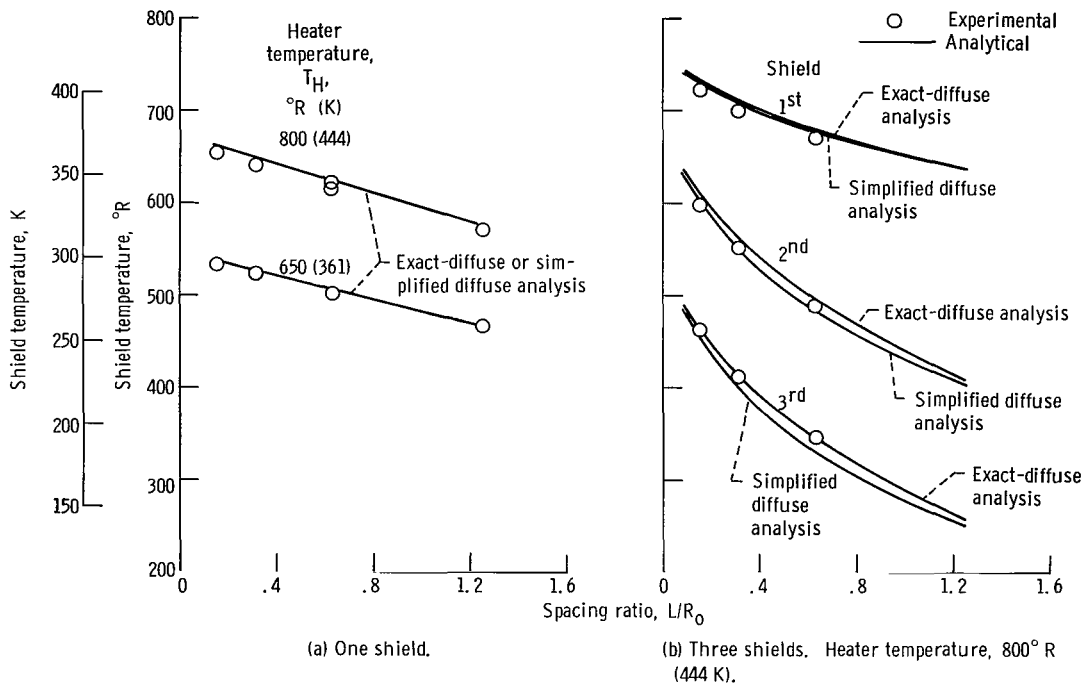
Figure 18. – Effect of spacing ratio on average shield temperatures for one and three intermediate-emissivity shields (shield II).

53

	Lateral conductance, $\frac{kt/R_0^2}{\text{Btu/(hr)(ft}^2)(°R); \ W/(cm}^2)(K)}$	Experimental heat flux, $(Q/A)_{ex}$ Btu/(hr)(ft²); W/m²	Analytical heat flux, $(Q/A)_{an}$ Btu/(hr)(ft²); W/m²	Shield
———— —	∞	---- ---	94.2; 297	---
O	4.25; 2.4x10⁻³	94.9; 299	--------	I
△	0.95; 5.4x10⁻⁴	92.6; 292	--------	III
◇	0.23; 1.28x10⁻⁴	93.4; 294	95.0; 300	IV
□	0.038; 2.13x10⁻⁵	94.3; 297	95.8; 302	V
▽	4.25x10⁻⁵; 2.4x10⁻⁸	97.6; 308	97.3; 307	VI
— — —	0	---- ---	98.4; 310	---

Exact-diffuse analysis

——— — Infinite conductance
——— Finite conductance
— — — Zero conductance

(a) High-conductance shield.

(b) Intermediate-conductance shield.

(b) Low-conductance shield.
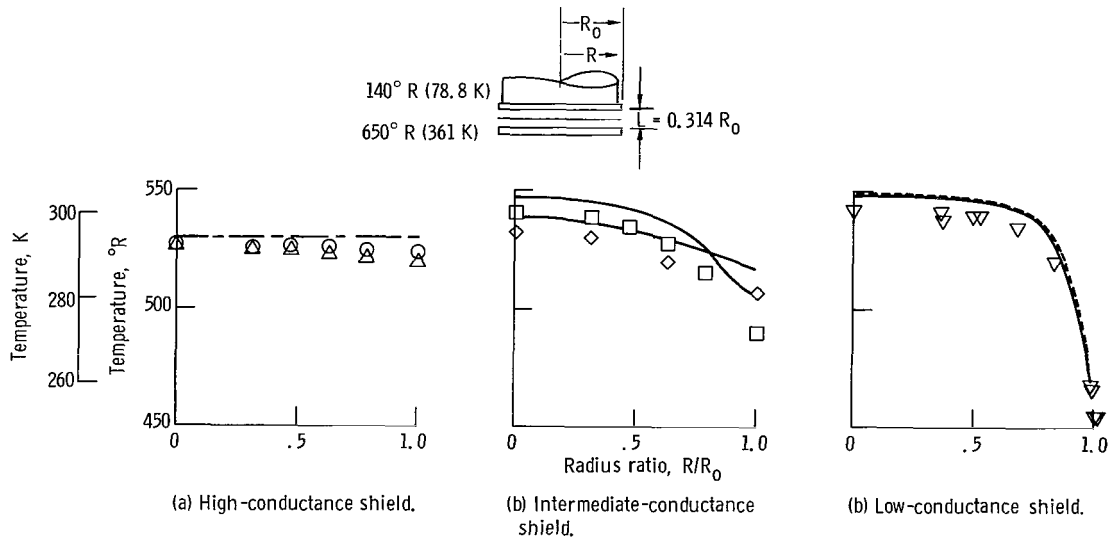
Figure 19. – Effect of lateral conductance on shield temperature profile and heat-transfer rate for single shield.

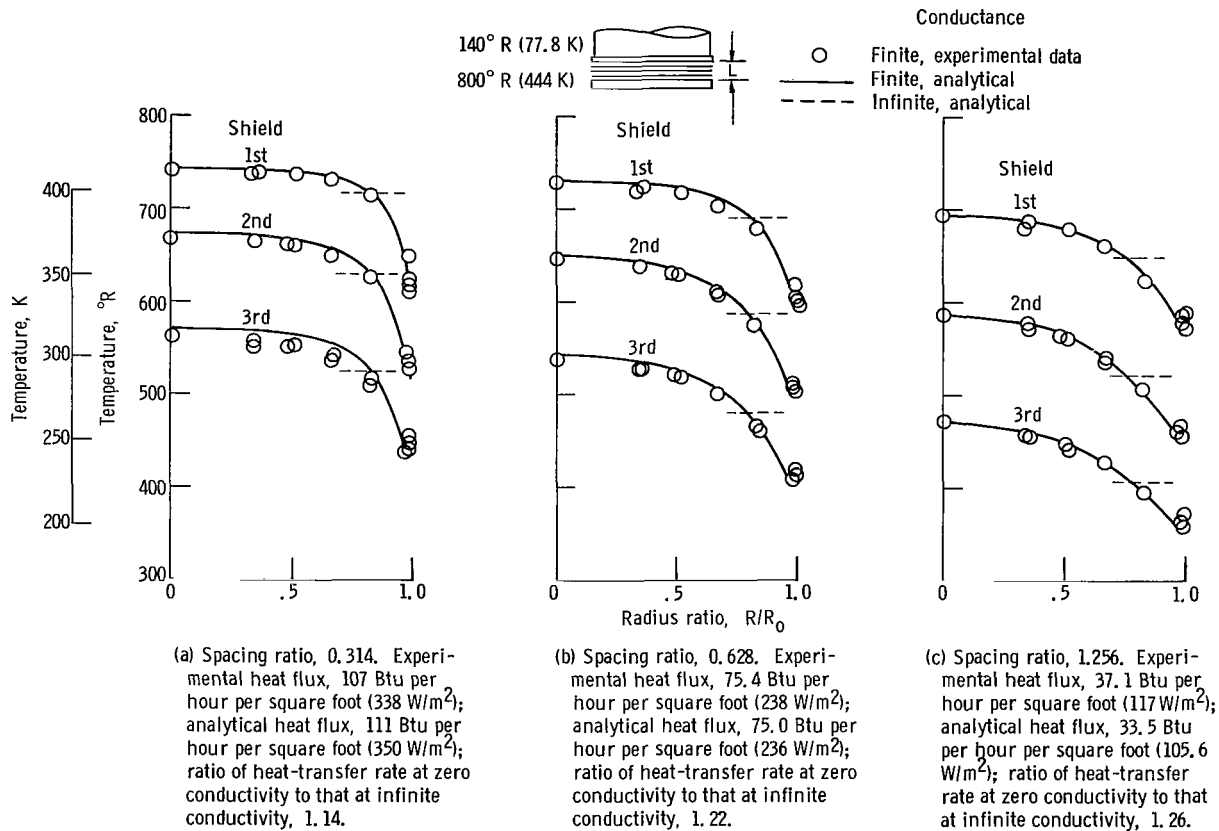(a) Spacing ratio, 0.314. Experimental heat flux, 107 Btu per hour per square foot (338 W/m²); analytical heat flux, 111 Btu per hour per square foot (350 W/m²); ratio of heat-transfer rate at zero conductivity to that at infinite conductivity, 1.14.

(b) Spacing ratio, 0.628. Experimental heat flux, 75.4 Btu per hour per square foot (238 W/m²); analytical heat flux, 75.0 Btu per hour per square foot (236 W/m²); ratio of heat-transfer rate at zero conductivity to that at infinite conductivity, 1.22.

(c) Spacing ratio, 1.256. Experimental heat flux, 37.1 Btu per hour per square foot (117 W/m²); analytical heat flux, 33.5 Btu per hour per square foot (105.6 W/m²); ratio of heat-transfer rate at zero conductivity to that at infinite conductivity, 1.26.

Figure 20. - Effect of spacing ratio on temperature profiles of three low-conductance shields (shield VI).

Figure 21. – Effect of targeting and spacing on shield temperature profiles (shields VI and VIII).
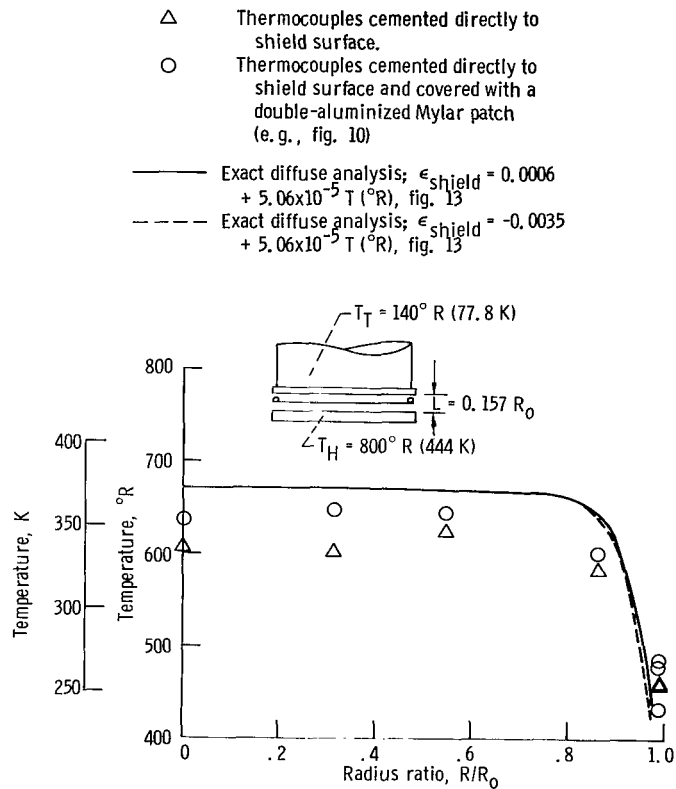
Figure 22. - Effect of thermocouple installation technique on local shield temperatures (shield IX). Analytical results assume shield is divided into 10 equal-area nodes and temperatures are plotted at mean area of each node. Heat flux (experimental), 10.4 Btu per hour per square foot (32.8 W/m^2).
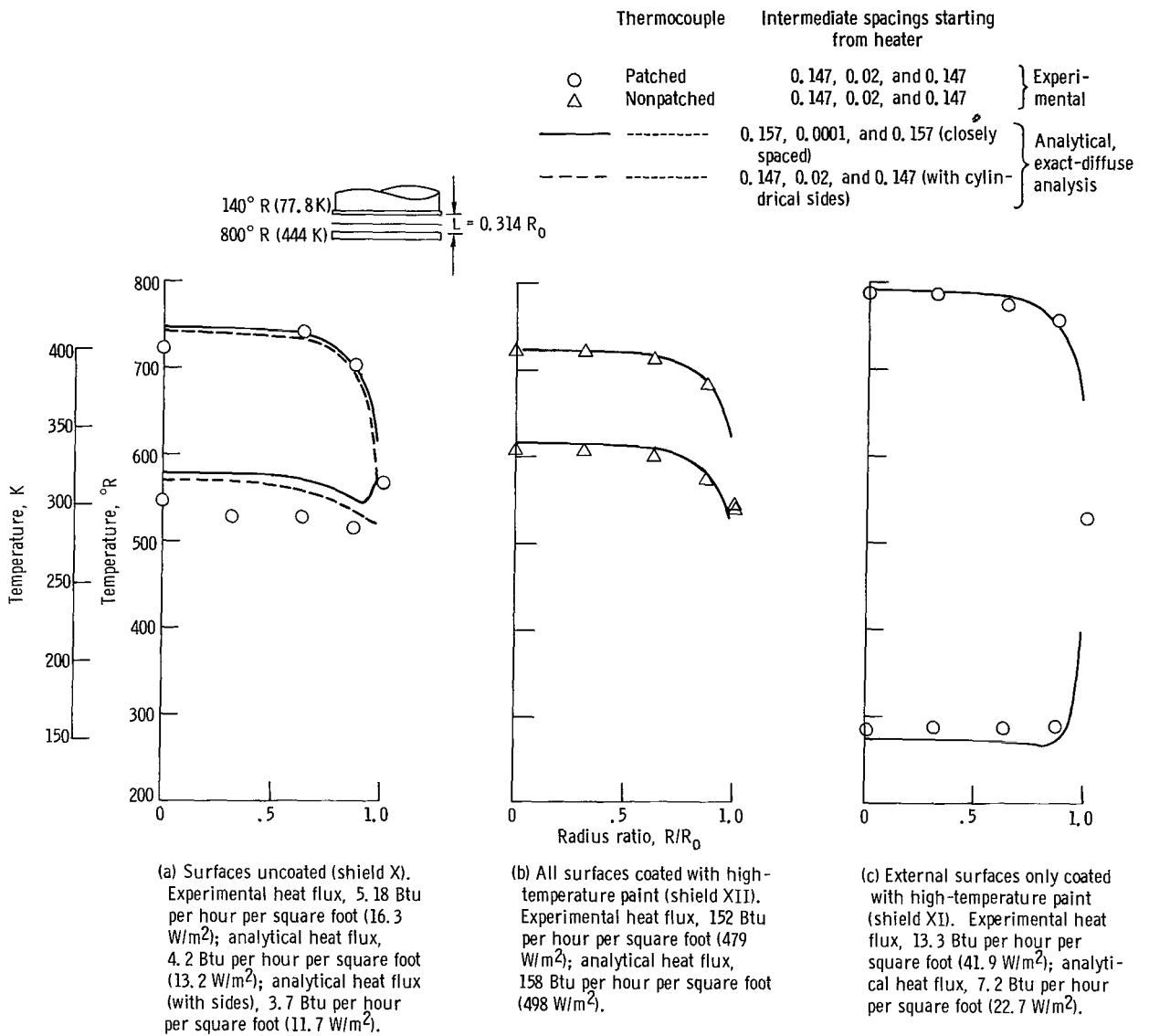
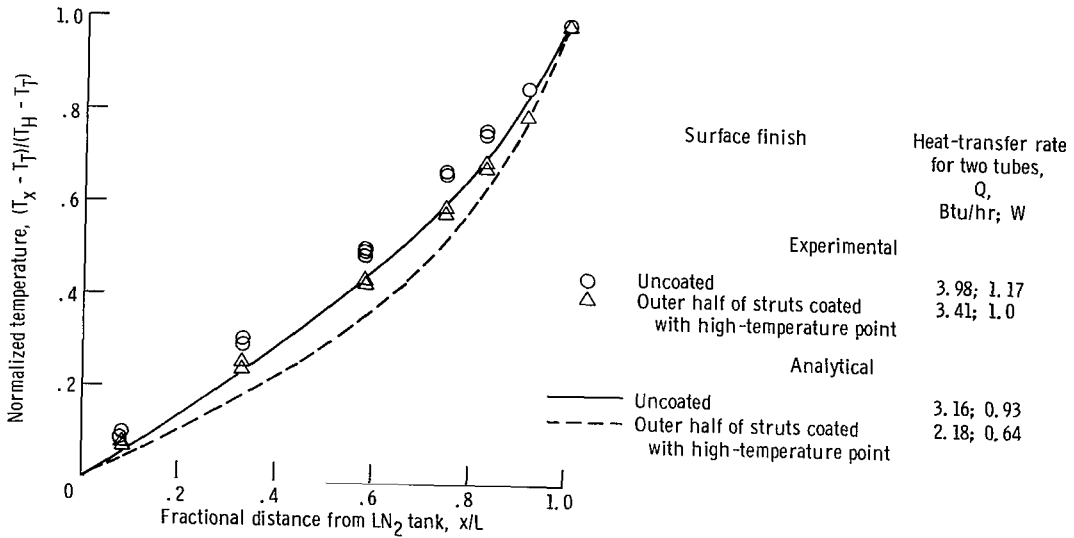Figure 23. – Temperature profiles for various surface properties on double-sheeted shields.
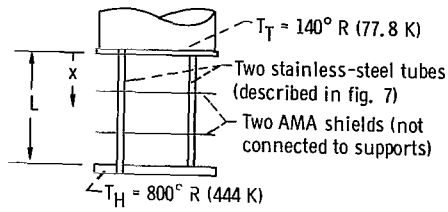
Figure 24. - Effect of external emissivity on temperature profile of 12-inch-long (30.5-cm-long) structural tube. Radiant heat transfer from shields <0.01 Btu/hr (0.00293 W).
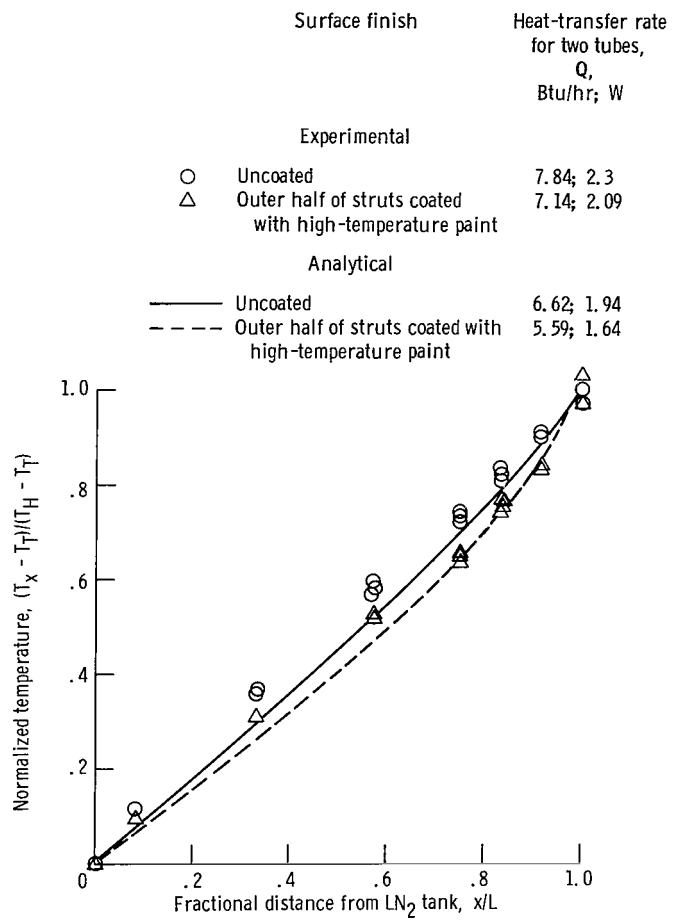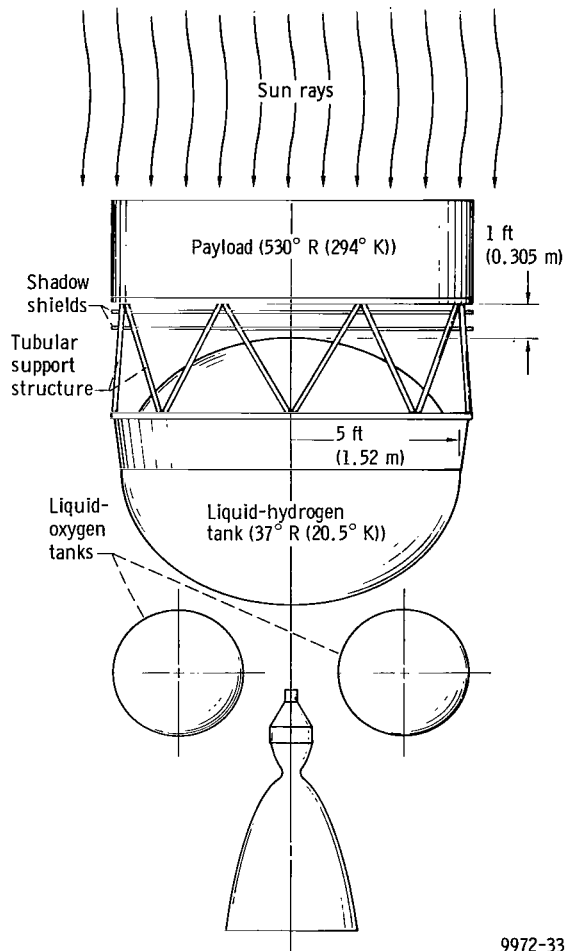
	Surface finish	Heat-transfer rate for two tubes, Q, Btu/hr; W
	Experimental	
O	Uncoated	7.84; 2.3
△	Outer half of struts coated with high-temperature paint	7.14; 2.09
	Analytical	
———	Uncoated	6.62; 1.94
— — —	Outer half of struts coated with high-temperature paint	5.59; 1.64

Figure 25. - Effect of external emissivity on temperature of 6-inch-long (15.2-cm-long) stainless-steel tube. Radiant heat transfer from shields <0.1 Btu/hr (0.0293 W).

Sun rays

Payload (530° R (294° K))

1 ft
(0.305 m)

Shadow
shields

Tubular
support
structure

5 ft
(1.52 m)

Liquid-
oxygen
tanks

Liquid-hydrogen
tank (37° R (20.5° K))

9972-33

Figure 26. – Schematic of hypothetical hydrogen-oxygen upper stage.
Structural details of vehicle below hydrogen tank are omitted for
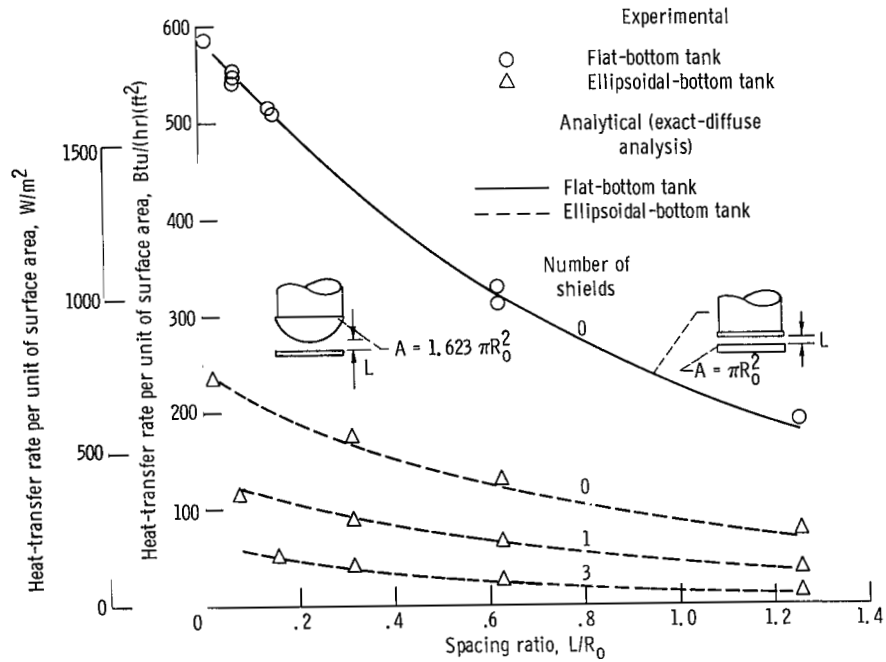clarity.

61

Figure 27. - Effect of tank shape on heat-transfer rate for several configurations (shield I). Surface area of ellipsoidal bottom is 1.623 times surface area of flat bottom. Heater temperature, 800° R (444 K); tank temperature, 140° R (77.8 K).
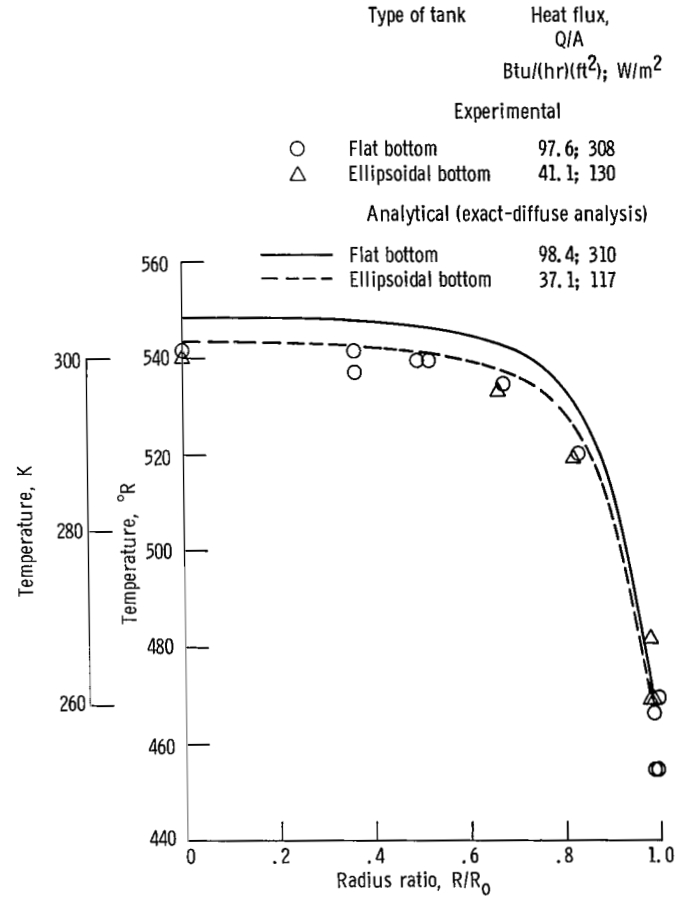

Figure 28. - Effect of tank shape on temperature profile of a single low-conducting shield (shield VI). Heater temperature, 650° R (361 K); spacing ratio, 0.314.
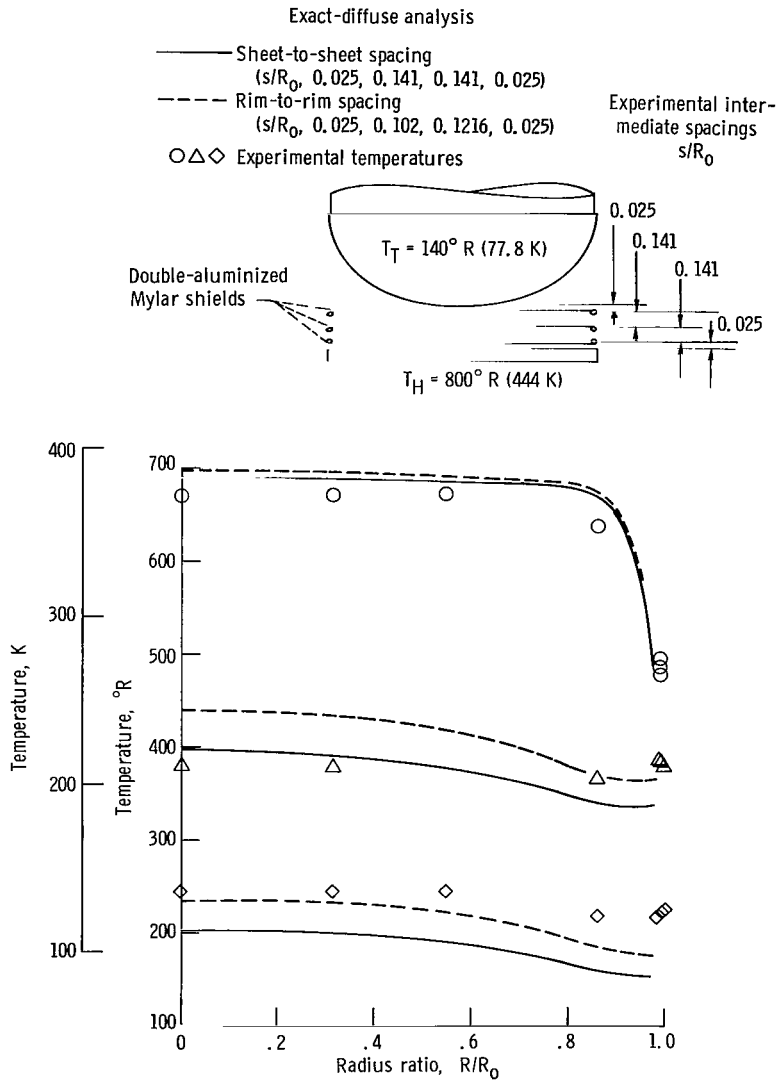
Figure 29. – Temperature profiles for three-shield configuration using doule-aluminized Mylar shields (shield IX). $L/R_0 = 0.332$.
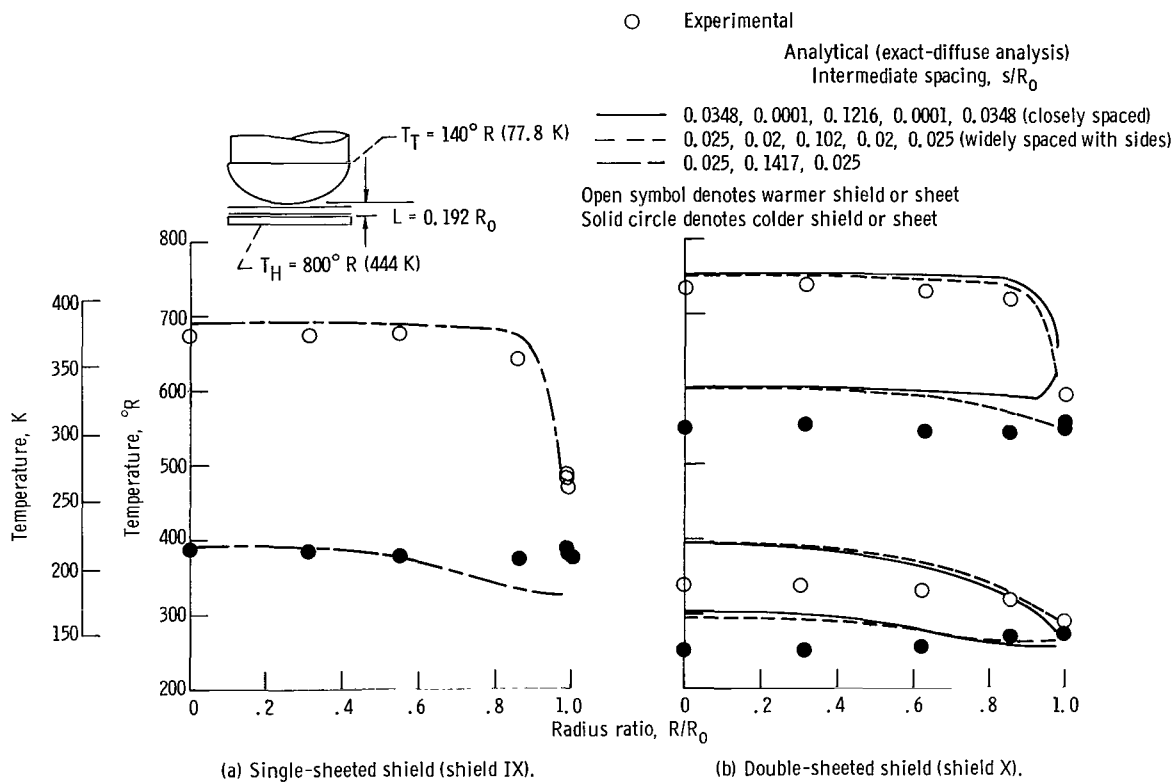
Figure 30. – Temperature profiles of single- and double-sheeted shields for scale-model configuration.
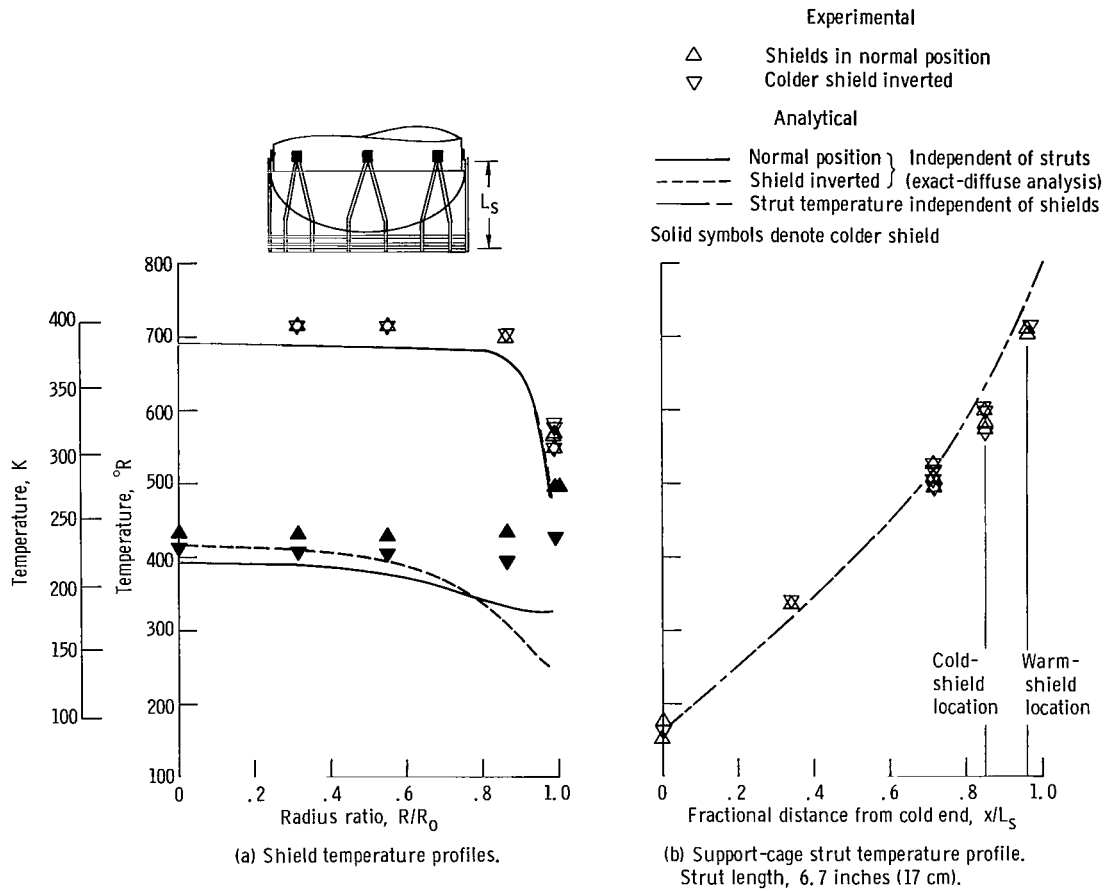
(a) Single-sheeted shield (shield IX).

(b) Double-sheeted shield (shield X).

Experimental

△ Shields in normal position
▽ Colder shield inverted

Analytical

——— Normal position ⎫ Independent of struts
- - - - - Shield inverted ⎰ (exact-diffuse analysis)
— · — Strut temperature independent of shields

Solid symbols denote colder shield

L_S

800
700
600
500
400
300
200
100

400
350
300
250
200
150
100

Temperature, K

Temperature, °R

0   .2   .4   .6   .8   1.0
Radius ratio, R/R_0

(a) Shield temperature profiles.

Cold-
shield
location

Warm-
shield
location

0   .2   .4   .6   .8   1.0
Fractional distance from cold end, x/L_S

(b) Support-cage strut temperature profile.
Strut length, 6.7 inches (17 cm).

Figure 31. – Shield and support-cage temperature profiles for pinned shields (shield IX). $L/R_0 = 0.192$.

65

Experimental

○   Shields freely suspended
△   Shields pinned
□   Shields welded
◇   Shields welded and targeted

Analytical

—————— Shields (independent of struts); exact-diffuse analysis
— —— Struts (independent of shields)

Solid symbols denote colder shields

(a) Shield temperature profiles.

(b) Support-cage strut temperature profiles.
Strut length, 6.7 inches (17 cm).
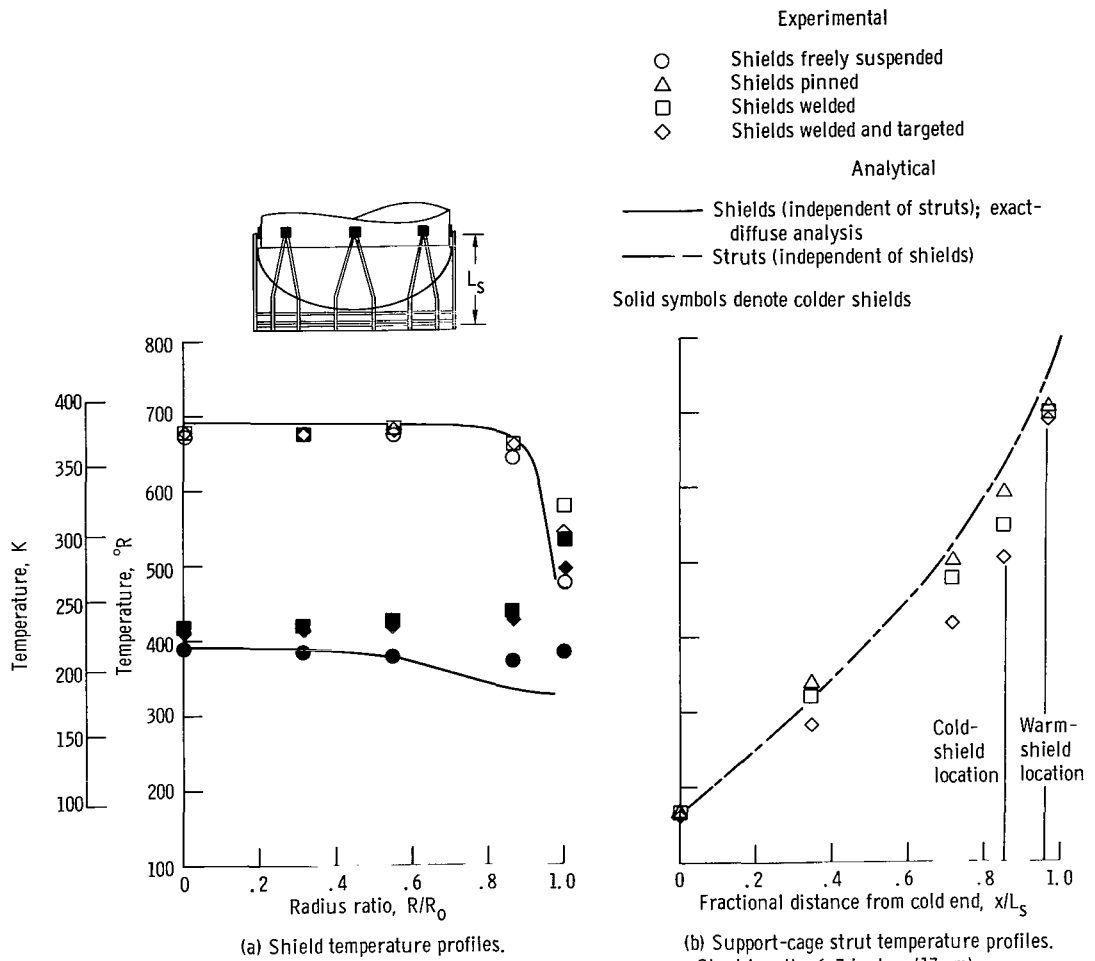
Figure 32. - Shield and support-cage temperature profiles for pinned, welded, and targeted systems (shield IX). $L/R_0 = 0.192$.
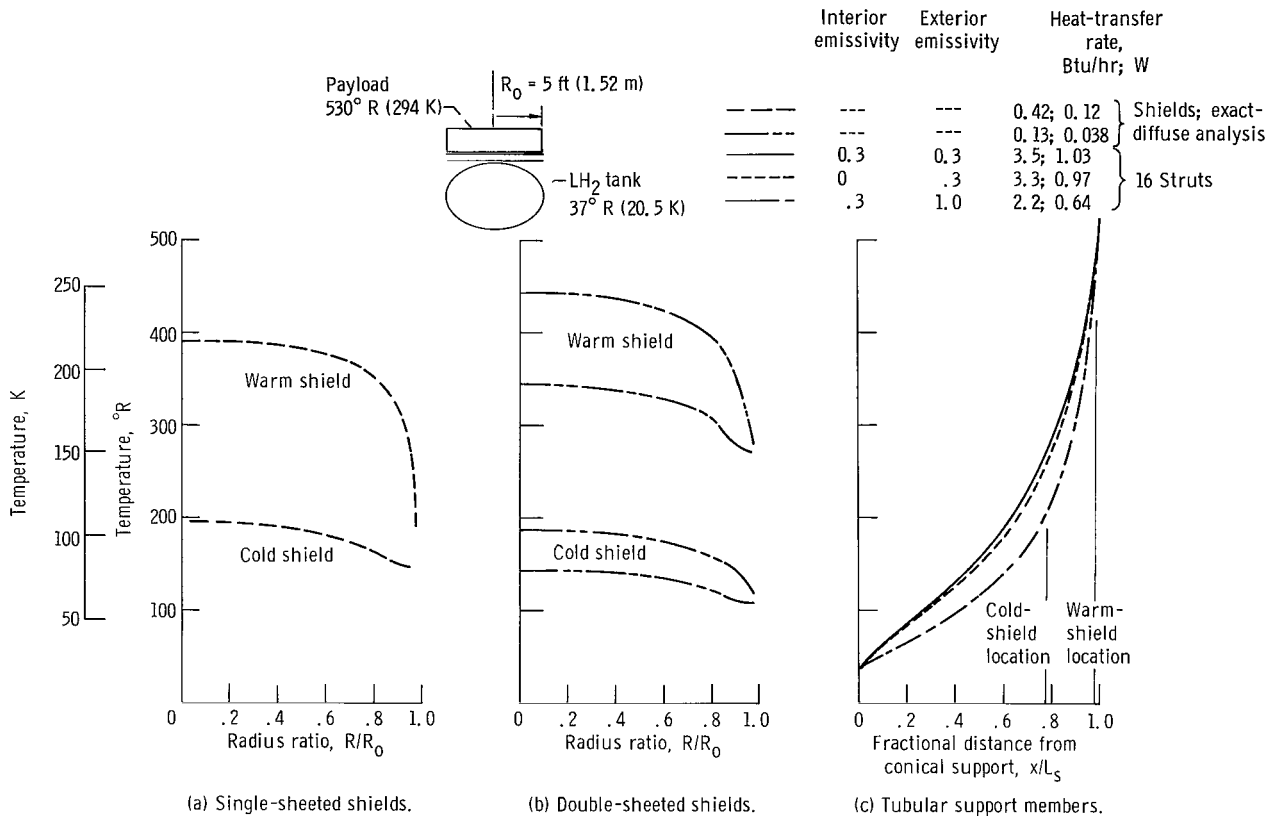
66

Figure 33. – Temperature profiles and heat-transfer rates for hypothetical shadow shield system. Payload, tank, and shield emissivity, 0. 03; support ring emissivity, 0. 3; lateral conductance, 0; spacing ratio, 0. 192.
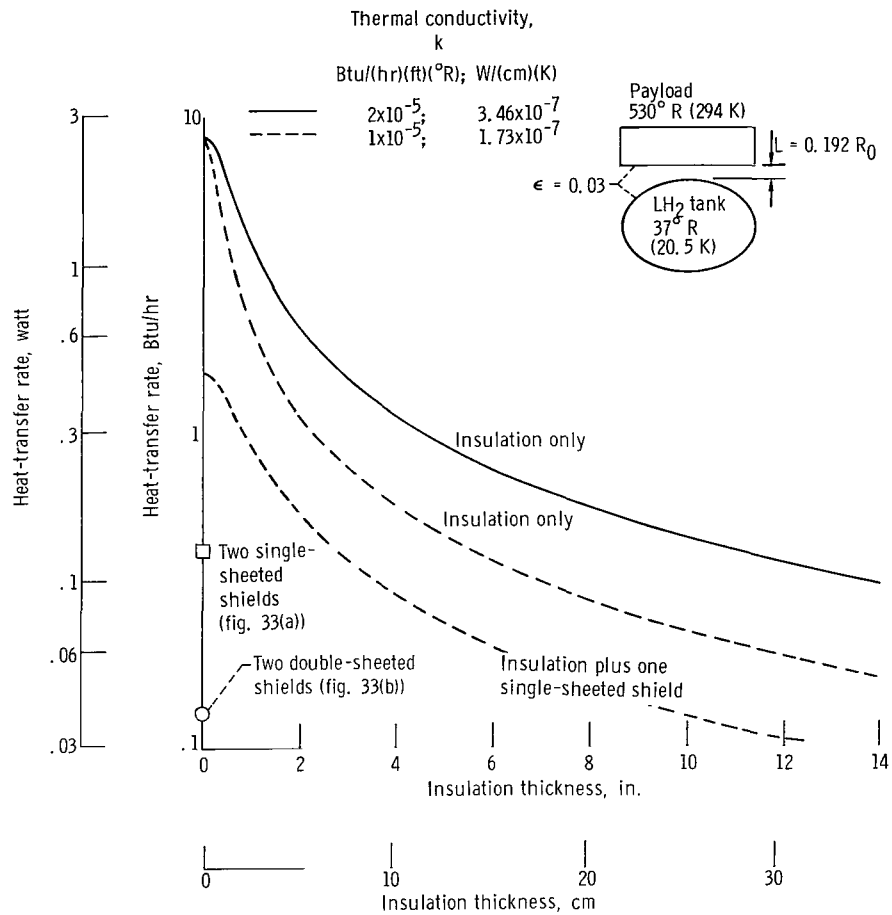
Figure 34. – Heat-transfer rate between payload and upper half of hydrogen tank of hypothetical vehicle as function of insulation thickness and thermal conductivity. Insulation surface temperature and thickness are uniform over entire upper surface of tank.
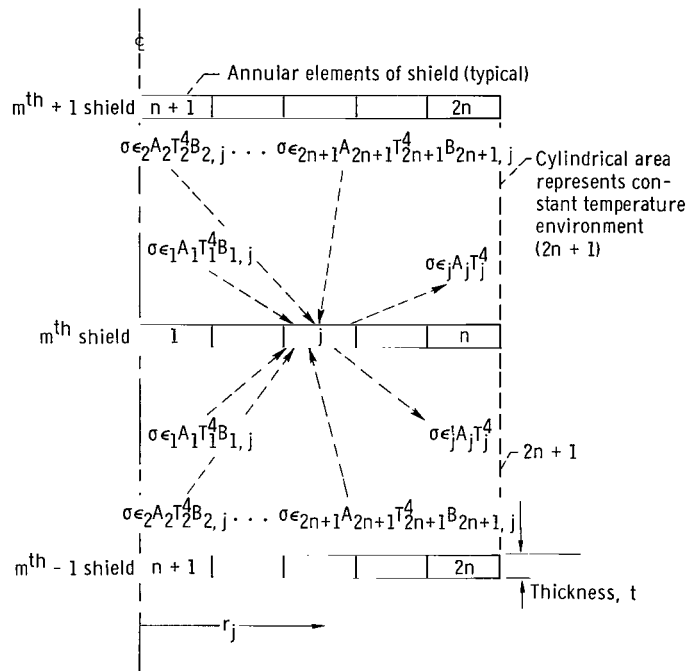
Figure 35. – Sketch showing radiant heat transferred to annular elemental area of shield.
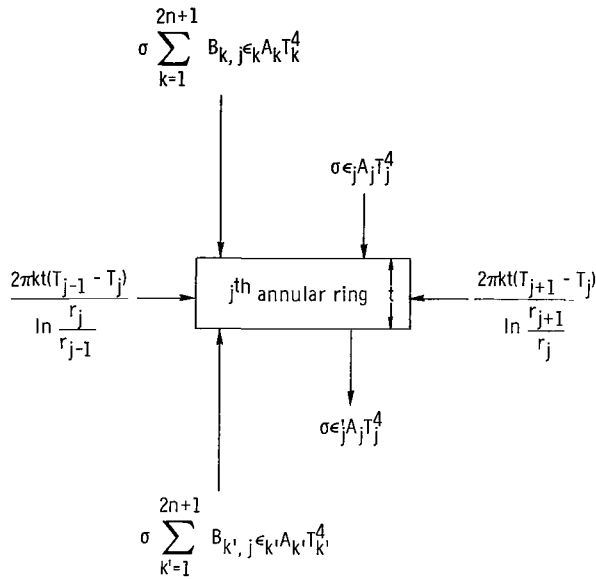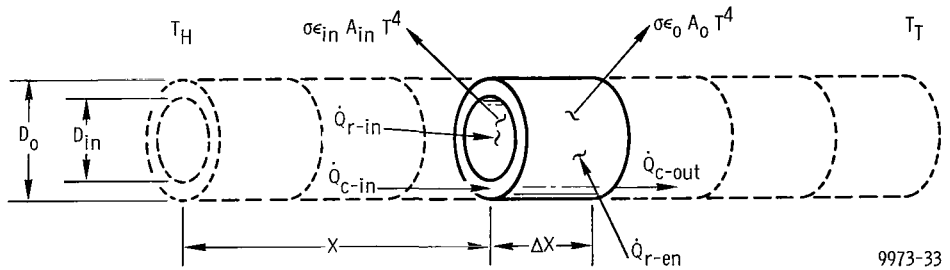
$$\sigma \sum_{k=1}^{2n+1} B_{k,j} \epsilon_k A_k T_k^4$$

$$\sigma \epsilon_j A_j T_j^4$$

$$\frac{2\pi kt(T_{j-1} - T_j)}{\ln \frac{r_j}{r_{j-1}}} \longrightarrow \boxed{j^{th} \text{ annular ring}} \longleftarrow \frac{2\pi kt(T_{j+1} - T_j)}{\ln \frac{r_{j+1}}{r_j}}$$

$$\sigma \epsilon_j' A_j T_j^4$$

$$\sigma \sum_{k'=1}^{2n+1} B_{k',j} \epsilon_{k'} A_{k'} T_{k'}^4$$

Figure 36. - Sketch showing conductive and radiant heat transferred into annular elemental area of shield. $A_j = A_j'$; $T_j = T_j'$.

$$\dot{Q}_{r\text{-}in} + \dot{Q}_{r\text{-}en} + \dot{Q}_{c\text{-}in} = \sigma T^4(\epsilon_{j,in} A_{j,in} + \epsilon_{j,o} A_{j,o}) + \dot{Q}_{c\text{-}out}$$

$$\sum_{l=1}^{k} B_{l,j} \epsilon_l A_l \sigma T_l^4 + \sigma T_{en}^4 \epsilon_o \pi D_o \Delta X + k \frac{\pi}{4}\left(D_o^2 - D_{in}^2\right)\left.\frac{dT}{dX}\right|_X = \sigma T^4(\epsilon_o D_o + \epsilon_{in} D_{in})\pi \Delta X + k \frac{\pi}{4}\left(D_o^2 - D_{in}^2\right)\left.\frac{dT}{dX}\right|_{X+\Delta X}$$

Figure 37. - Sketch and heat balance for tubular strut. Heat input equals heat output; l is total number of elements in enclosure, including tube ends.

9973-33